8-25-2014

3D Imaging and Investigation of Failure and Deformation in Thermal Barrier Coatings Using Computed X-ray Tomography

Navid Asadizanjani
University of Connecticut - Storrs, naveedasadee@gmail.com

Abstract

3D Imaging and Investigation of Failure and Deformation in Thermal Barrier Coatings Using Computed X-ray Tomography

Navid Asadizanjani,PhD

University of Connecticut, 2014

Zirconia-based thermal barrier coatings are widely used as a protection of the underlying metal from the hot gas stream in turbine engines TBCs are made of four layers including: a ceramic top coat, thermally grown oxide (TGO), a metallic bond coat, and super alloy substrate and each layer has different thermo mechanical properties. To investigate the behavior of TBC systems using traditional imaging techniques such as, SEM micrographs taken from serial sectioning, white light interferometry, optical coherence tomography, mid infrared reflectance imaging, and thermal wave imaging will not give the opportunity of performing non-destructive evaluation and 3D imaging simultaneously. Three-dimensional non-destructive information allows a unique opportunity to follow the progression of crack damage. A number of fundamental questions can be addressed with such data which include: a) Is there a correlation between the bond coat interface geometric features and the location of the cracks? b) What are the shapes of bond coat cracks as needed for modeling? c) Do large cracks grow faster than the smaller cracks? d) What is the nature and role of crack linking in damage progression? e) What is the relationship between the geometry change at the hidden bond coat to ceramic interface and the ceramic free surface and can the free surface geometry change that is more easily measured be used to assess the extent of bond coat interface geometry change? Bond coat geometry change can in some cases be used to predict failure offering a potential non-destructive inspection method. This

work will demonstrate the feasibility of 3D non-destructive imaging for obtaining the desired information by X-ray tomography. Then tomography will be used to address the fundamental questions listed above. The present work first establishes a method for monitoring the progression of cracking in TBCs using x-ray tomography and then uses this information to answer the important questions a-c above. Also a partially successful attempt to develop confocal microscopy for the same purpose will be briefly described.

3D Imaging and Investigation of Failure and Deformation in Thermal Barrier Coatings Using Computed X-ray Tomography

Navid Asadizanjani

B.A., Khaje-nasir-toosi University of Technology, **2008**

M.A., Amir Kabir University of Technology, **2010**

A Dissertation

Submitted in Partial Fulfillment of the

Requirements for the Degree of

Doctor of Philosophy

at the

University of Connecticut

2014

APPROVAL PAGE

Doctor of Philosophy Dissertation

3D Imaging and Investigation of Failure and Deformation in Thermal Barrier Coatings Using Computed X-ray Tomography

Presented by

Navid Asadizanjani, B.S., M.S.

Major Advisor _____
Eric H. Jordan

Associate Advisor _____
Brice Cassenti

Associate Advisor _____
Michael Renfro

University of Connecticut
2014

Contents

Chapter 1 Introduction 10
1.1 Imaging Techniques 12
1.2 Crack investigation techniques 18
Chapter 2 Confocal Microscopy 21
2.1 Experimental Methods 21
2.2 Confocal Microscopy Results 24
Chapter 3 X-ray Tomography Technique 27
3.1 Experimental procedure 30
3.1.1 Acquisition of X-ray projections 31
3.1.1 Source and detector 32
3.1.3 Use of Energy Filter to Enhance Transmission 34
3.1.3 Optimizing number of Projections 35
3.2 Image Reconstruction 37
3.3. Image processing 41
3.3.1 Image Segmentation 41
3.3.2 Quantitative analyses of TBC layers and repeatability verification 42
3.3.3 Detecting Pores from Cracks 44
3.4 Optimized X-ray Tomography Technique 44
3.4.1 Optimizing Sample size 45
3.4.2 Optimizing Image acquisition Parameters 50
3.4.3 Optimizing the pixel size and X-ray counts: Trade-off with tomography time 51
3.4.4Optimizing Repeatability: Image Registration 55
3.5 Results 59
3.5.1 Interfacial Surface Geometry Change 62
3.5.2 Crack evolution 62

Chapter 4 Crack Analyses 65
4.1 Visualization of TBC internal structures 65
4.2 Cracks behavior 73
4.3 Crack correlation with TGO 77
4.5 Correlation between bond coat and top coat surface geometry 78
Chapter 5 Conclusion and future work 81
Chapter 6 References 88

Table of Figures

Figure 1-1 EBPVD on the left and Air Plasma Sprayed top coat structures on the right. 10
Figure 1-2-Imaging techniques used for thermal barrier coatings 17
Figure 2-1- Prepared sample for confocal microscopy 21
Figure 2-2- Fluorescence mode of the microscope 22
Figure 2-3- Reflection mode of the microscope 23
Figure 2-4- Serial sectioning process 24
Figure 2-5- Typical result of confocal microscopy 25
Figure 2-6- Volume view of confocal microscopy images 26
Figure 3-1-Four layers of the imaged TBC system 31
Figure 3-2-Image of the inside of Micro XCT 400 (left) and Schematic of principle of Micro CT tomography (right) 31
Figure 3-3- (a) and (b) Issue with flat disks where the positioning of source and detector is affected (c) one of the proposed remedies 33
Figure 3-4 – Transmission percent with and without filter 35
Figure 3-5-Effect of Number of Projections on the quality of imaging TBCs- Region of Interest: Cracks in TBC 37
Figure 3-6-Effect of the number of projections on the quality of images- Region of interest: Borders of layers 37
Figure 3-7-Center Shift Effect on Image Quality 38
Figure 3-8- Optimization for beam hardening value 39
Figure 3-9-Effect of smoothing filter on image quality 40
Figure 3-10-a)Image taken from X-ray, b) segmented image, c) 3D surface generated 42
Figure 3-11- Repeatability analysis of bond coat surface parameters before and after thermal cycling with X-ray CT compared with stereo photogrammetry 43
Figure 3-12– Six different sample sizes selected for experiments. (All dimensions in mm) 47
Figure 3-13– Virtual slice of reconstructed images for samples of figure 1 (all samples are shown after 25 hours of thermal cycling at 1121 C) 49
Figure 3-14- Zeiss Versa 510 inside view 51
Figure 3-15- X-ray counts relation with respect to the distance between source and detector 52
Figure 3-16- Stitched image, 3D representation of smaller scans (a), and stitched (b) 55
Figure 3-17- Pre-registration of 2D projections in 90 degrees 56
Figure 3-18 - post-registered reconstructed images 57
Figure 3-19-Repeatability check of the XCT, Surface generated for same sample in two scans in (a) and (b), top surface is separated from each scan (c) and (d), two surfaces are aligned (e) 58
Figure 3-20- Line tortuosity change for a) bond coat and b) top coat using X-ray tomography 59
Figure 3-21- Correlation coefficient between top coat and bond coat profiles before and after thermal cycling 61
Figure 3-22- Segmented TBC image 62
Figure 3-23- Crack propagation tracking 63
Figure 3-24- b) crack tracking parameters 64

Figure 3-25– Crack and pores observation in a segmented image 64
Figure 4-1- A progression of X-ray tomography images of sample (a) from thermal cycling experiments 66
Figure 4-2-Cracks and TGO presentation of sample (a) during multiple cycling 68
Figure 4-3– Separated cracks before linking in the 50 hour thermally cycled sample at 1121ºC 69
Figure 4-4– Cracks linked and selected as a single crack 70
Figure 4-5 – a) Crack growth in a 3 by 3 size sample, b) Presenting TGO surface curvedness with respect to cracks location for 80 hours sample 71
Figure 4-6 – Side view of cracks on sample (d) after 80 hours of thermal cycling at 1121 73
Figure 4-7– Faster crack growth seen in area closer to TGO 74
Figure 4-8– Crack linking to the TGO grown at top of the peaks 75
Figure 4-9– Quantified crack growth behavior 77
Figure 4-10-Correlation between crack and TGO seen in some specific areas 78
Figure 4-11– Top surface separation of TBC and BC for correlation analyses 79
Figure 4-12– Tortuosity values for bond coat and top coat selected profiles and correlation between them 80

Chapter 1 Introduction

Zirconia-based thermal barrier coatings are widely used as a protection in hot gas stream in turbine engines, primarily to reduce metal temperatures and reduce high temperature oxidation and corrosion [1]. These coatings allow turbines to operate at higher temperatures which can improve the efficiency while also lowering the substrate temperature that can enhance the durability of the engine [2]. TBCs are made of four layers including: a ceramic top coat, thermally grown oxide (TGO), a metallic bond coat, and super alloy substrate and each layer has different thermo mechanical properties,.

There are two deposition methods for the ceramic top coat: Electron Beam Physical vapor Deposition (EBPVD) and Air Plasma Spray (APS), Fig. 1-1. Although the thermo mechanical properties of EBPVD TBCs are usually better in terms of performance comparing, APS TBCs cost much less. Both types eventually spall off after thermal cycling,

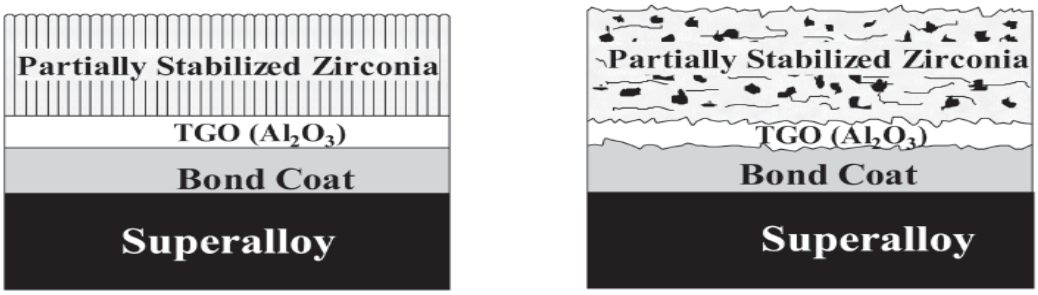

Figure 1-1 EBPVD on the left and Air Plasma Sprayed top coat structures on the right.

Failure of TBCs in this multilayer complex system will result in exposure of the metal layer under the top coat to the extremely hot gas, which can produce premature failure. The most important reasons among other failure reasons are: a) stresses associated with thermal expansion mismatch between the metal and ceramic, b) Bond-coat oxidation, and c) bond coat geometry changes due to rumpling d) sintering of the TBC e) exposure to contaminants such as calcium

magnesium aluminum and silicates (CMAS) Surface geometry changes of the interface between bond coat and top coat in TBCs is one of the contributing causes of failure which has been investigated in different types of TBCs. Rumpling behavior of platinum modified NiAl and MCrAlY bond coats has been both investigated in previously [2- 22]. 2D and 3D parameters are well established to state the geometry changes such as: RMS roughness, line tortuosity, area ratio, which is the ratio of the true area of a surface to the projected area [12, 13, and 21] skewness, kurtosis, and bearing area ratio [27]. Dynamic behavior of these parameters before and after heating treatments has been investigated on bare bond coat samples. Serial polishing and imaging is also used to quantify the surface parameters change [23], but it is a tedious process and errors are highly possible when matching the images of each section with the one of the region on either side of it. It should be also noted that although 3D information will be collected from this method, it is a non-repeatable and destructive method which eliminates the opportunity to investigate the same region of interest as the sample is cycled. Hence this method will not allow observation of the shape evolution of an individual feature. Although bond coat surface geometry has been studied, the top coat surface geometry change associated with surface underneath and the correlation between the two have not yet been investigated. The present work includes such an investigation and feasibility of establishing such a relationship between the ceramic top coat 3D surface change and the subsurface bond coat/TGO interfacial surface change. Correlating the two surfaces can enable a novel non-destructive evaluation method or TBCs by measuring the top coat surface geometry change to learn about the damaging geometry changes of the bond coat ceramic interfaces a potential nondestructive evaluation technique for life prediction. In addition, we seek to image and record the 3D geometry and evolution of cracks in the top coat and correlate the crack evolution to asperities in the interfacial geometry such as

mountains and valleys. Direct observation of the evolution of such cracks will provide fundamental information about the nature of the damage process and ultimately lead to better damage models. Important information would include: a) is the crack initiation location correlated with the initial bond coat TBC interface geometry. b) What are the shapes of bond coat cracks as needed for modeling c) What role does interface shape change paly in the location and growth of cracks. d) Crack linking is known to be a feature of the damage, what is the geometric relationship; that needs to occur for cracks to link up? e) What is the relationship between the geometry change at the hidden bond coat to ceramic interface and the ceramic free surface and can the free surface geometry change that is more easily measured be used to assess the extent of bond coat interface geometry change?

1.1 Imaging Techniques

There are various types of imaging techniques that can be used for surface characterization and cracks investigation in thermal barrier coatings. These methods are enumerated such as, Mid infrared imaging, traditional cross section scanning method, white light interferometry, optical coherence tomography, confocal photo simulated micro spectrometry, stereo photogrammetric, and X-ray computed tomography.

Serial sectioning: The most common technique still used is the traditional method of characterizing the cross sections with serial polishing, which is a widely available process [12-14]. Although this process widely available, it is a time consuming process and there is a high possibility of error and challenge in order to match the images of each cross section with the one before and after it. The most undesirable part of this process is the fact it is a destructive method in which the region of interest cannot be imaged repeatedly after each thermal cycles. Each cross section will result in a 2D profile which is a part of the surface under investigation. This

technique can be used for any type of TBCs regardless of the coating deposition type or thickness.

White light interferometry: Using white light scanning interferometry one can get three dimensional surface parameters of a free surface including the bare bond coat. This is a nondestructive method which has been used to characterize bare bond coat NiPt samples to check the rumpling [17,21]. In this method white light is coming from the source and will be radiated in two branches to the object and the reference mirror. The phase shift due the path length difference between the absorbed rays from the reference mirror and the rays coming back from the object will generate after some processing the final three dimensional image of the sample. Although the obtained result is a three dimensional image which gives the x,y, and z information of the object , we are getting the information of the top surface of the object only. It has been found that when the sample has a very rough surface the light is trapped in the surface and does not reflect back to the camera which makes it a challenge to get meaningful images from MCrAlY bond coat samples. This is due to the fact that the light rays will not be reflected back to the camera from overhangs or dimples behind peaks.

Stereo photogrammetry: Stereo photogrammetry is a three dimensional technique for imaging which is well developed to image the surface parameters using scanning electron microscopy [24]. Height and depth information are extracted based on the Piaezessi algorithm in this method, which is commonly used in photogrammetry for earth mapping. Three different micrographs from different angles of the same area has to be taken to generate x,y, and z data of the surface. In order to make sure the same area is imaged, a fiducial “L” shaped mark has been carved on the samples using Focused Ion Beam machine. This mark helps to match the images taken from different angles.

SEM images have high resolution and high signal to noise ratio comparing to optical images. In addition there is no contact in SEM imaging which makes it suitable for rough surfaces. Since the images are taken from three different angles the overhangs on peaks or valleys can be also well detected. Due to the mentioned benefits of this method, it can be used for bare MCrAlY samples which are rougher comparing with the NiPt aluminized bare bond coat samples [25-32]. The image acquisition stage consists of acquiring images of the same area, matching the images taken from different angles, and finally extracting the third dimension. Although the image reconstruction process is computationally intensive, but using the fast computers it will be possible. This is also a nondestructive way of imaging which gives the opportunity to record the free surface parameters in 3D and track the changes of the same area as the samples are thermal cycled multiple times. However, this method is limited to bare bond coat samples and the effect of the TBC and possible changes on the ceramic top coat are not yet known.

Confocal Laser Microscopy: This is another optical imaging technique in which the optical resolution and contrast of the micrographs are increased using a pin hole which eliminates the out of focus light coming from the object [25, 31]. The major difference of this technique with the traditional wide field microscopes is the use of the point illumination and the pinhole in front of the detector which cancels out the out of focus signals and only the light generated from the focal plane can be detected. The depth of the observed volume depends on the movement of the microscope and the thickness of the focal plane is related to the numerical aperture, and the objective lens. Depending on the absorptivity of the samples laser can penetrate and reflect back to take images or florescence can be stimulated and detected. As the objects get more pores, laser will be subject to large scattering losses and even multiple scattering that can cause non focal plane information to leak into the images causing the method to fail at some level of scattering.

A material with higher absorption coefficient will also limit the depth of imaging. So in order to make a large stack of two dimensional images it is required to polish or cut the region which is imaged and look at the part underneath where the laser was not able to penetrate before polishing. With this method the technique will be counted as a destructive method but the images resolution is much better than the general optical microscopy [39].

This method has been previously used in researches to visualize cracks and bare bond coat surface structures in TBCs but three dimensional results are not presented appropriately, specially, for cracks or pores volumes which were imaged [32-38].

X-ray Computed Tomography: X-ray tomography is widely used for imaging in medical fields. The imaging concept is based on acquisition of two dimensional projections which will be used to reconstruct the three dimensional image. It is very challenging to get meaningful images using the micro CT for TBCs. There are many parameters which have to be modified and optimized o obtain good results and in addition extensive post processing is required to convert the image to more meaningful quantitative 3-D information.

In this method the object is located between the X-ray source and the detector. X-rays will be passed through the object and will be absorbed by the detector. Object will be rotated about the vertical axis of the sample and one two dimensional projection will be taken for each angle. In previous work the possibility of using the X-ray in thermal barrier coatings was investigated however further research is required to analyses the results and reconstruct the three dimensional images [40-46]. Due to the nature of this technique where the X-rays will pass through the objects, images quality does not depend on the complexity of the sample geometry. Three dimensional images can be viewed and analyzed in any of the three planes of view. Overhangs

and roughness can be detected as long as the features size is of the same size range as the detector's pixel size or larger. A different X-ray attenuation coefficient for each material in the periodical table also helps to separate the layers of the sample during the 3D reconstruction. Material integrity, surface characterization parameters, and volume analyses on pores and cracks can be done on the images depending on the resolution of the images. This is a nondestructive imaging technique which can do multiple imaging of the same region of interest at different times during thermal cycling tests and track the progression of damage. The challenges of this technique will be discussed in the next section as well as the preliminary results and analyses as development of this method is the primary topic of this thesis.

Other techniques: There are also other techniques such as mid infrared reflectance imaging was first used by Eldrige based on IR reflection from TBC coupons to estimate the crack growth and delamination [47]. Clarke used piezospectroscopy to acquire 2D images of delamination for electron beam physical vapor deposition coupons [48], although it is possible to roughly estimate where the crack is located using these images but they can neither demonstrate crack shape in 3D nor can they be used for APS samples. Ray et. al. studied crack propagation behavior under bending load. They have used SEM micrographs and sectioning process in their studies and investigated the importance of porosities as stress raisers and reasons for crack initiation [49]. Thermo graphic monitoring of crack evolution was also studied as a nondestructive technique by Capelli [50], where they benefit from the change in thermal diffusivity of TBC coupon's due to the crack growth and delamination. Chen et. al. also studied crack nucleation and TGO growth with 2D SEM micrographs under the effect of peroxidation and proposed the existence of a power law relation between the maximum crack length in TBC and TGO [51].

In the work in this thesis, research confocal imaging micro CT imaging techniques are selected due to the ability of the methods to visualize the cracks and their evolution in thermal barrier coatings before and after series of thermal cycles, as well as the investigation of the possible correlation between the top surface of the top coat with the top surface of the bond coat in both APS and EBPVD samples. We will try to derive a quantitative relation between the roughness and other surface parameters of the mentioned two surfaces in order to control them for aero or any other reasons. This will help to monitor the top coat surface which is easy to access instead of the bond coat and find the changes in the bond coat using the data from surface changes of the top coat. TBC imaging methods are presented in Fig. 1-2.

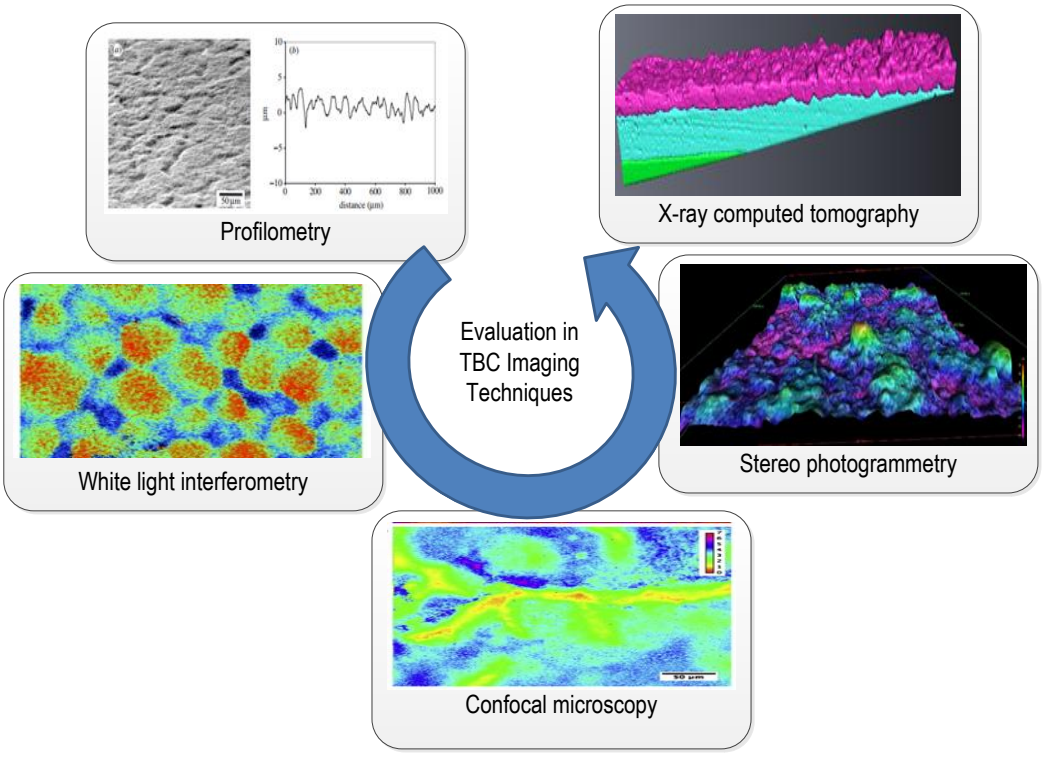

Figure 1-2-Imaging techniques used for thermal barrier coatings

1.2 Crack investigation techniques

This work will investigate the feasibility of non-destructive imaging for thermal barrier coating systems. It will also provide a valuable source of data for Finite Element modeling on the cracks to show if the previous assumption for the crack shape, behavior and growth are valid or not. In [53, 59] the modeling shows that the delamination cracks form in the TGO layer over the bond coat and the maximum stress in the TBC were found to be between the peaks and valley of the TGO asperities. In some researches crack behavior is modeled using linear elastic fracture mechanics [54-58], but TBCs seem to have inelastic behavior. In [58] cracks are assumed to grow inside the TGO and over peaks of the bond coat asperities where there are large values for residual stresses based on the simulation. In [59] a sine curve used for modeling the roughness using a visco-plastic model and FEM output considered in four points: peak, above peak, valley, and above valley. It was found out that the failure occurs by cracking parallel to the coating surface in the top coat layer for an APS TBC sample. Cracks are suggested to initiate and grow near the tip of the interface in the TBC due to stress distribution map and high residual stress in that area in TBC [61, 62]. Bond coat peaks are also suggested in [63, 64] for early cracking and the increase of the growth for the cracks when TGO gets to a critical thickness. Elastic and visco-plastic models are compared in [65], where it is shown that elastic stresses can be up to three times larger, and cracks are simulated over the TGO interface on the peaks and between peak and valley. Effects of residual stress from the thermal spraying process are also investigated in [66, 67] and TBC peak region are suggested as probable regions for micro-cracks to appear. In this research we will try to first provide the methodology to acquire 3D images of TBC samples and also provide this type of information for APS TBC samples and address a number of fundamental questions:

a) What is the common shape for most of the early cracks in TBCs?

b) Is the crack initiation location correlated with the initial bond coat TBC interface geometry?

c) What role does interface shape change paly in the location and growth of cracks.

d) Crack linking is known to be a feature of the damage, what is the geometric relationship; that needs to occur for cracks to link up?

e) What is the relationship between the geometry change at the hidden bond coat to ceramic interface and the ceramic free surface and can the free surface geometry change that is more easily measured be used to assess the extent of bond coat interface geometry change?

Confocal microscopy and X-ray computed tomography are selected due to their potentials in detecting features and the goals of this research in order to visualize the three dimensional shapes of cracks, and pores inside the thermal barrier coating layers as well as surface parameters and roughness. Although X-ray tomography enables us to visualize the features properly, small cracks and pores might not be captured well if they are very small. For this reason confocal microscopy will be used as a compliment to the X-ray tomography. Confocal microscopy was investigated first due to the fact that a suitable X-ray tomography device (160 KV source) was not initially available. The use of confocal microscopy for TBC was a new idea that proved possible but the section depths that were possible were smaller than desired. Accordingly after a demonstration of the feasibility and limitations of confocal microscopy for TBCs we focused on X-ray tomography. We therefor present confocal microscopy and X- ray tomography in separate

sections as to method and results and discuss then together in the discussion and conclusion section.

Chapter 2 Confocal Microscopy

As mentioned in the previous section, confocal microscopy has been used for imaging the surface parameters and roughness in TBCs. Three D fluorescence imaging by confocal microscopy is widely used in biology but it is not yet used to present three dimensional images of cracks and pores in TBC.

2.1 Experimental Methods

In order to capture the cracks and pores, Spurr resin epoxy with a very low viscosity of 6×10^{-2} Pa·s was used as an embedding material for vacuum impregnation [26] of our TBCs. This epoxy enables sufficient penetration into the material using with a vacuum furnace. Epodye (Struers) which is a fluorescent (Rhodamine) dye is also added to the epoxy to enhance the contrast of crack and voids using a confocal laser microscopy. The epoxy was be poured on the specimen in the mold and it will be placed in the vacuum furnace. The chamber was evacuating to 30 inHg and opened to the atmosphere pressure again so that the air pressure helps the infiltration, this process is repeated three times to help better penetration the epoxy in the specimen. After this step the chamber temperature was set to 70^{o} C and cured in 8 hours. The APS sample in epoxy is presented in figure 2-1.

Figure 2-1- Prepared sample for confocal microscopy

The microscope used was a Nikon model A1R which uses a 488nm laser to excite the fluorescent dye inside the specimen. Due to the nature of the top coat ceramic it is found out that the laser cannot penetrate more than 5 microns deep into the material. Therefore, image stacks of 20 slices are taken for every 5 micron and the three dimensional image can be reconstructed using multiple stacks by polishing the sample. To control the polishing process for taking 5 micron of the material Vickers hardness device is used, figure 2-2 and 2-3.

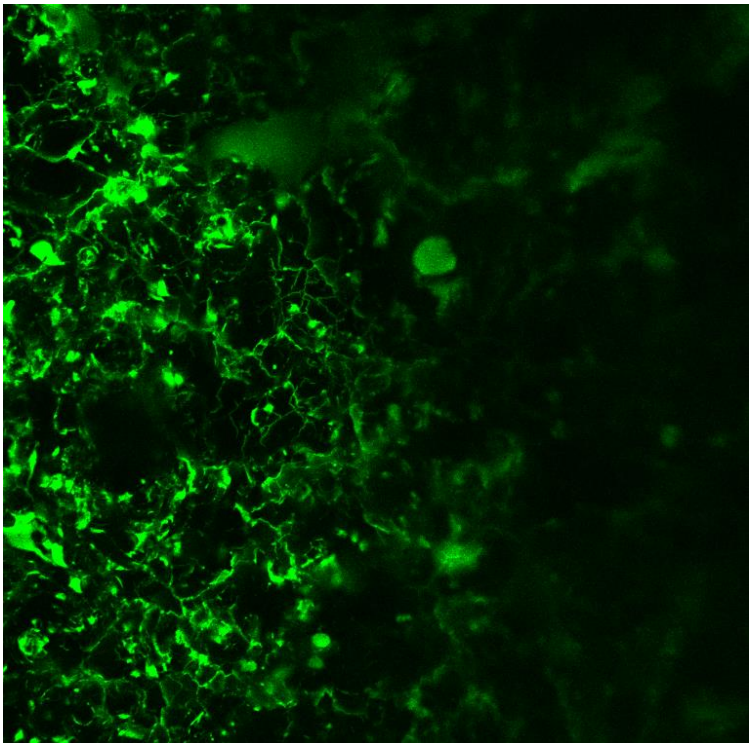

Figure 2-2- Fluorescence mode of the microscope

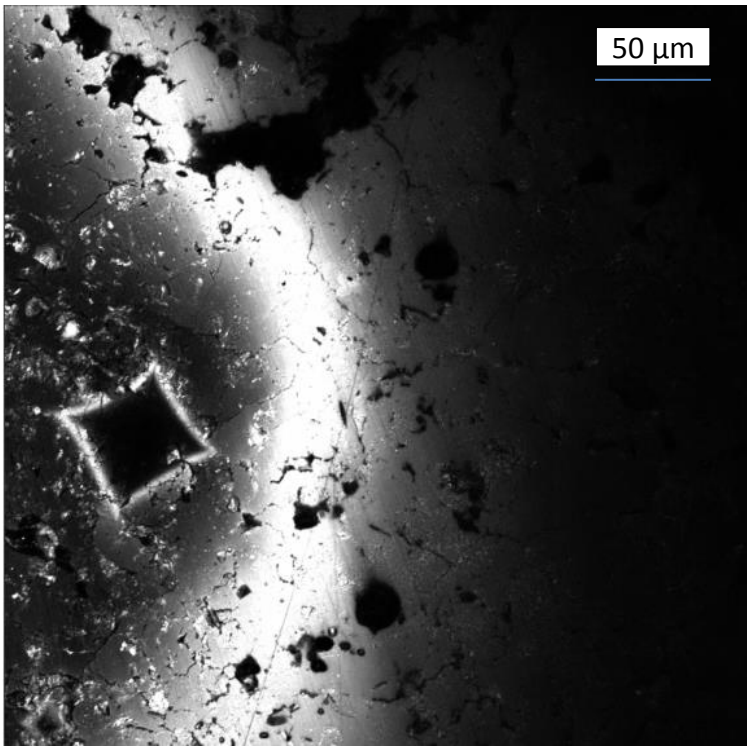

Figure 2-3- Reflection mode of the microscope

Using the relation between the diameter of the Vickers sign on the material and the tip angle, the depth can be easily calculated. So, one spot of the specimen is chosen for putting Vickers mark and check the polishing depth by checking the diameter of the Vickers mark repeatedly during the polishing. It has been found out that using the 3 micron diamond solution and polishing with 5 newton forces for 3 minutes will polish off about 5 micron from the specimen. This process can be repeated multiple times to generate a volume image of the specimen. This method collects much more information per section compared to simple sectioning because the full 3D image of the 5 micron slice is recorded compared to a single plane in standard sequential sectioning. Serial section process is presented in Figure 2-4.

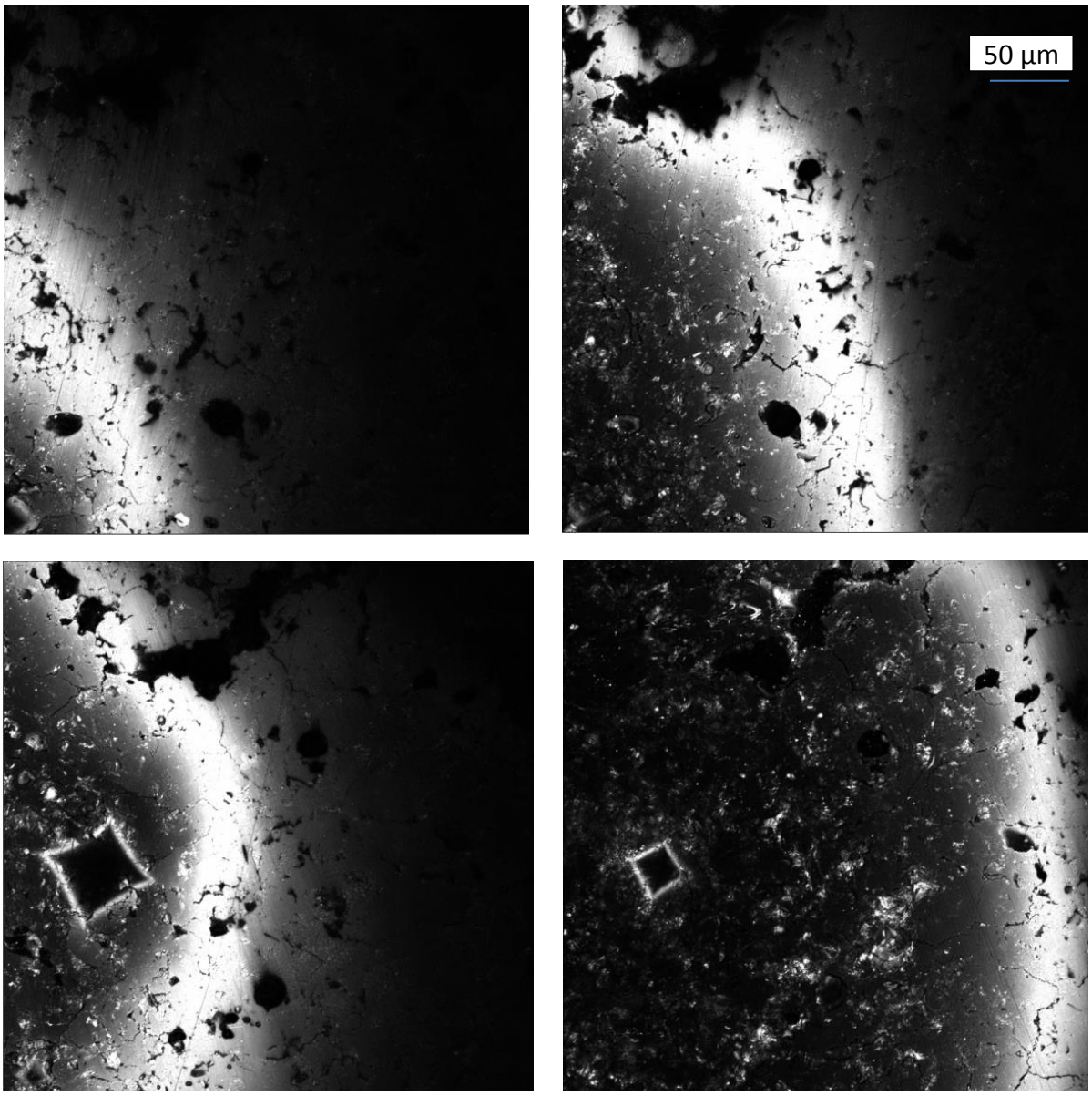

Figure 2-4- Serial sectioning process

2.2 Confocal Microscopy Results

Since the laser 488 nm is just exciting the fluorescent dye so the image is basically showing the pores and cracks, Fig. 2-5, which can be analyzed and the shape of cracks observed after thermal cycling of the specimen. The only problem with this technique is that, it is destructive which does not allow tracking the evolution of a crack over multiple heat treatment process.

In order to observe the top coat ceramic completely the process should be repeated multiple times to cover the whole thickness of this layer. Although the process can be accomplished on the side cross section in horizontal direction, where all three layers, top cot, bond coat, and substrate will be visible in each stack of images but it is recommended to take images vertically as side polishing of the specimen might end up at an angled cross section, due to the presence of different layers with different mechanical strength in this direction, which poses issues in matching the last image taken from the previous stack with the first image taken from the new stack after polishing each time. Figure 2-5 shows a typical result from confocal microscopy

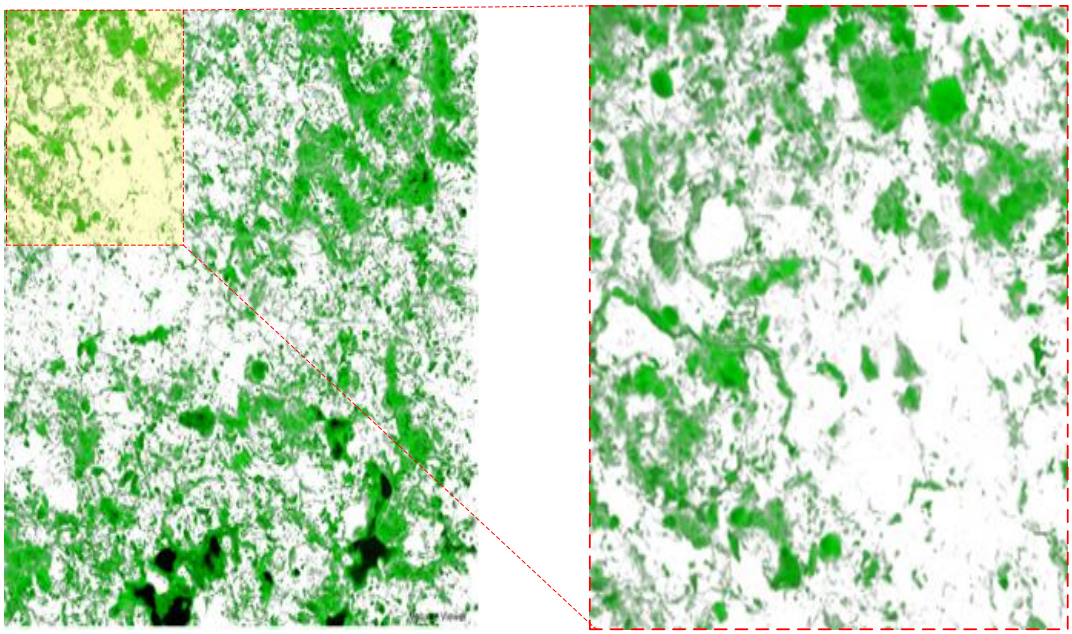

Figure 2-5- Typical result of confocal microscopy

Figure 2-6 shows reconstructed volume view of confocal laser microscopy images of the pores.

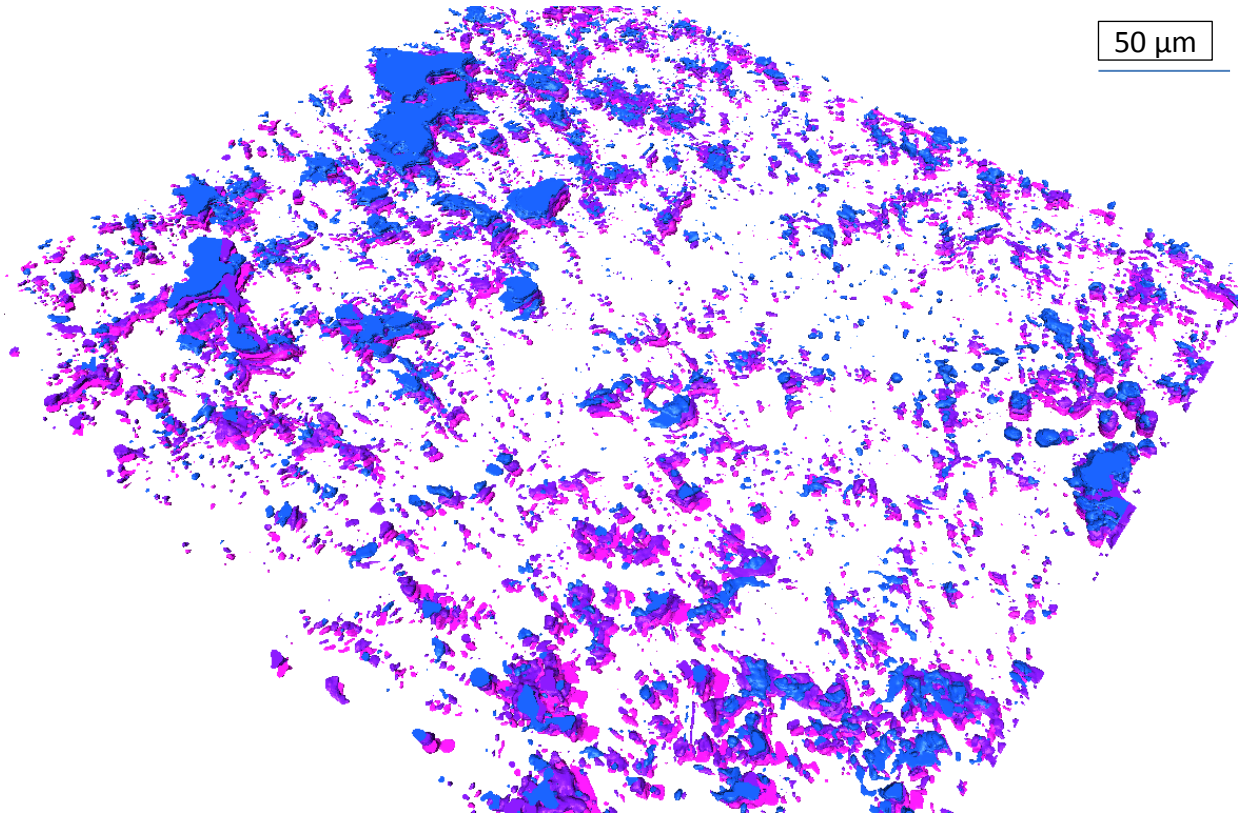

Figure 2-6- Volume view of confocal microscopy images

Because of the limitations of this method and the effort required it was not pursued further and x-ray tomography was used for the remainder of the work.

Chapter 3 X-ray Tomography Technique

Since confocal microscopy is not a nondestructive method, using X-ray computed tomography was used in this research for imaging crack evolution. As was mentioned earlier it is a highly challenging process to acquire successful images from TBCs using micro CT especially because of the strong attenuation of x-rays by the metal and ceramic in the sample. The University of Connecticut recently acquired a Zeiss X-ray tomography machine with a 160 kv and a second with a 90 Kv source which has been available for about 5 years. The 160 KV source is much more suitable for imaging highly absorbing TBC samples compared to the 90 KV source machine. There are challenges during the X-ray imaging and offline challenges for three dimensional image reconstruction from the 2D acquired projections. We will briefly go through the online challenges in X-ray imaging:

- The distance between source, sample, and detector: since the source is not a perfect point source blurry edges have to be minimized by changing these distances while the dealing with attenuation coefficient which limits the sample to detector distance in order to have enough X-ray counts to form a good imager.

- Material attenuation coefficient: materials with high attenuation coefficient which are not in the region of interest need to be thinned down in order to increase the detected x-ray counts and hence the image quality.

- Filters: low energy X-rays which will result in noise of the images can be eliminated by using proper filters.

- Exposure time: working with flat samples will require using exposure time tables which will assign specific exposure time for every angle during the imaging adjusting the

exposure time to longer times for regions of greater thickness to obtain sufficient x-ray counts to form consistent low noise images in a reasonable length of time. Another suggestion for dealing with flat samples is to cut a thin strip of these samples which has the interested features in it.

- Number of projections: details level on the final 3D image is directly related to the number of 2D projections. An optimum value has to be set to optimize the level of details and the costs of imaging consisting of imaging time and file size.

2D projections need to be processed using several tools to correct the imperfections of the images before 3D reconstruction. These parameters are called as off line parameters and are as following:

- Center shift: movement of the specimen center of rotation during imaging on the scale of micrometer is highly possible due to the temperature change in the room or other reasons, which will end up in an offset between the center of the specimen and the detector. A computed correction for this will help to compensate for the offset and retain sharper edges in the images.

- Beam hardening: attenuation of the x-rays will have relatively greater for the X-rays transmitted through the center of the specimen compared to the ones transmitted through the edges. This will result in a non-uniform brightness of the image even where the material is known to be the same material. A computed beam hardening correction will help to make more uniform the received X-ray spectrum which will correct the brightness of the image.

- Smoothing filter: this filter optimizes the resolution of the image versus image noise. Micro CT images can be used either for surface characterization or material integrity and crack analyses. It is highly recommended to smooth the image using a higher kernel size filter in order to get clear surfaces with high signal to noise ratios, but low values for kernel size will give us the details of the image with less smoothing and lower signal to noise ratio. Depending on the analyses type this kernel sized can be selected for the filter to suit the specific purpose in a given image analysis.

When the imaging process is completed, Avizio Fire 8.0 was used to assign material for each pixel of each layer segment). Depending on the quality of the images there are different filters to use to further improve the quality of the segmentation.. Depending on the shapes of the features in the image any of the view planes can be used to labeling and assign material. Each slice will be then considered separately to assign the material and generate the 3D surface by combination of all the slices next to each other.

This process will be used on images both APS and EBPVD TBCs to investigate the surface parameters, crack imaging, and the correlation between the top coat and bond coat surfaces during thermal cycling of the specimens. Thin strips will be cut off from the coupons and tested and imaged multiple times to precede the investigation.

When the images are segmented and labeled all the image information is converted to x,y,z data, which can be used to do various analyses. In order to do a 2D comparison of the profiles between top coat and bond coat different slices can be chosen from these surfaces. To make sure the profiles are independent of each other, a minimum distance is set between each two slices equal to the characteristic wavelength of the surface that is about the size of the particles. Line

tortuosity or area ratio can be also extracted from the data and results will help to see whether or not the rumpling is occurring on the bond coat and top coat and how they are related with thermal cycles and coating types.

3.1 Experimental procedure

Disk-shaped (2.54 cm in diameter and 0.32 cm in height) specimens consisting of a 150-micron thick low pressure plasma sprayed MCrAlY (31Ni–Bal. Co–21Cr–8Al–0.5Y wt. %) bond coat were used for this study. Bond coat samples were plasma sprayed using Metco 204 XCL powder with 7% YSZ to the thickness of almost 100 microns. The super alloy was initially machined to thicknesses of one millimeter from the original 3 mm in order to allow the X-ray to penetrate through the samples. Figure 3-1 shows the front view of a sample shown as a 2D slice of a thermally cycled sample with all four layers present. In order to investigate the possibility of recording small changes in TBCs after thermal cycling, specimens were heat treated employing a CM rapid cycle furnaces with an automated stage elevator. Furnace cyclic oxidation test in air consisted of a 10 minute heat-up to 1121 ºC followed by a 45-minute dwell at 1121 ºC and a 5-minute forced air cooling. To investigate the possibility of characterizing change in TBC at the early stages where only small changes occur, heat treatment was only done for only 40 cycles which was previously shown to be only 10-20% of the life of such samples[7].

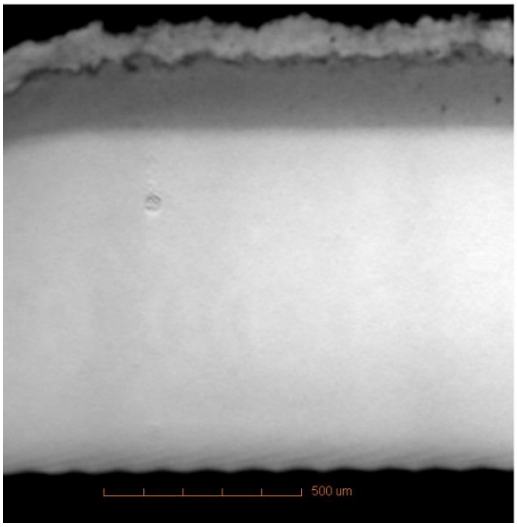

Figure 3-1-Four layers of the imaged TBC system

3.1.1 Acquisition of X-ray projections

Micro X-ray tomography (Micro CT) was performed using Zeiss Micro XCT 400. Figure 3-2 shows a schematic of the principle of Micro CT imaging (right) along with an image of the inside of the machine (left) showing x-ray source, detectors and sample stage in the cited instrument.

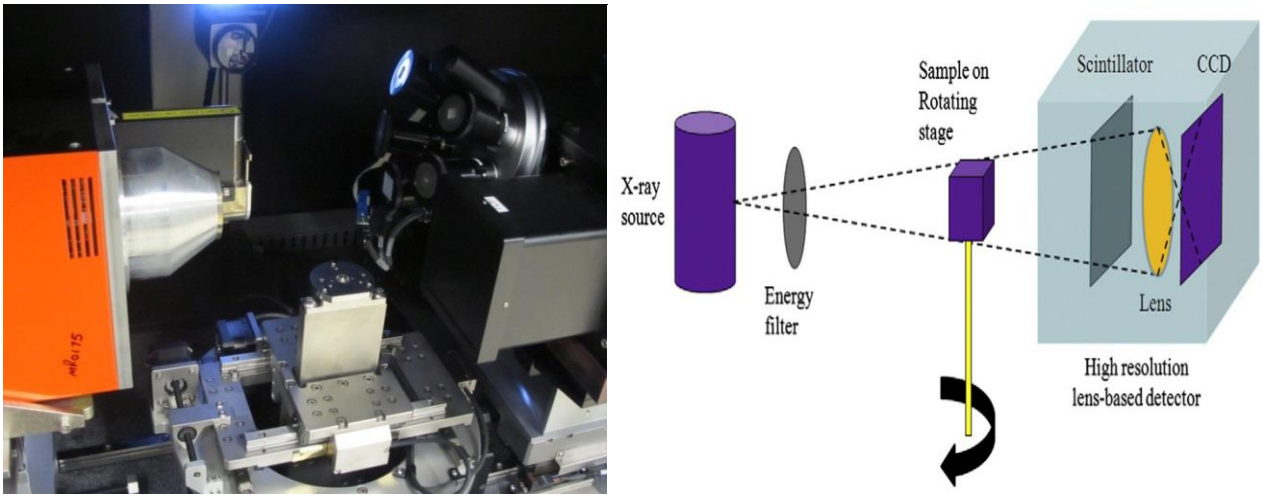

Figure 3-2-Image of the inside of Micro XCT 400 (left) and Schematic of principle of Micro CT tomography (right)

As shown in the figure, the principle of Micro CT is based on acquiring several 2D X-ray projections at different rotating angles [35]. The projections are then reconstructed to create 3D image of the sample by providing stack of 2D reconstructed slices. There are many control parameters in image acquisition needed to be optimized for a successful tomography including: position of the source and the detector, x-ray exposure time, voltage and power of the source, the objective of the detector and number of images for tomography. The following section of the papers will discuss these parameters based on the parts involved;

3.1.1 Source and detector

Due to high x-ray attenuating characteristics of the materials used in TBC systems [36], the maximum voltage and power must be used for the imaging which for the cited instrument is 160kv and 10 watts resulting in the current to be almost 88 micro-amps. There are several detector objectives offered by the instrument based on the pixel size and field of view. For thermal barrier coatings, the authors have used 10X objective which has a pixel size of less than 2 microns with a field of view of almost 2 by 2 mm. Higher objectives have resulted in less than a millimeter of field of view and lower ones do not provide the resolution required for the analysis of TBC in terms of surface geometry change.

It is desirable to have the source and detector as close as possible to the sample during tomography. If the samples are used as disks, the source and detector are to be positioned far enough to avoid collision with source/detector at all rotating angles. This phenomenon has been shown in Figure 3-2 (left) where the detector and source position have been positioned based on the sample orientation at an angle which has the maximum X-ray path length which creates an unwanted distance at the angle of minimum x-ray path length.(right)

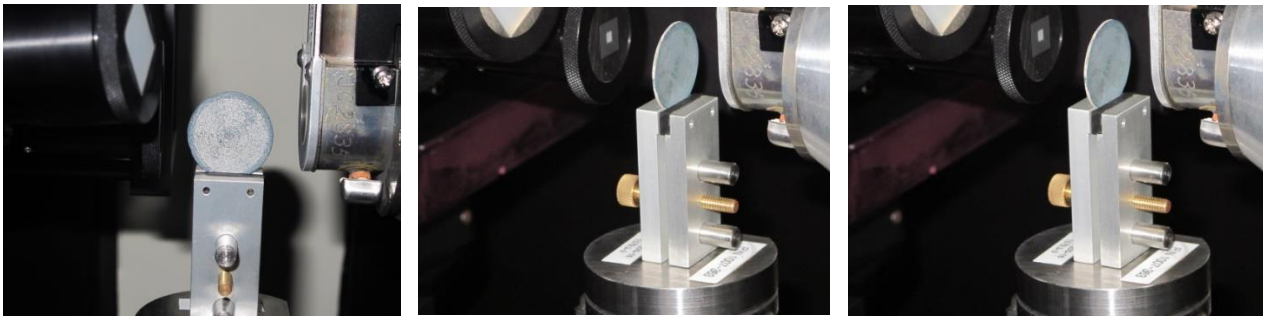

Figure 3-3- (a) and (b) Issue with flat disks where the positioning of source and detector is affected (c) one of the proposed remedies

This results in considerable loss of X-ray counts. For instance, in samples of this study, the number of x-ray counts were 6000 in the center of the image for a given exposure time when source and detector were close to the sample. However as they are moved to accommodate the disk diameter the X-ray counts for the same exposure time dropped down to 1500, a reduction by a factor of 4. This leads to a necessary increase in the exposure time which can result in a 4 times longer tomography increasing the chance for sample movement during tomography and forcing error in results. Also if the exposure is increased excessively, the detector can be maxed out by more than 60,000 counts (Detector's limitation) resulting in misrepresented values of transmission which will be the essential information for the reconstruction algorithm.

To overcome this issue, two possible remedies were tried. Firstly the samples are kept as disks however an exposure time factor correction table was used. Using this table, the exposure time will be multiplied by a factor ranging from 1 to 4 as the angles were changing from 0 to 90 degrees (Figure 3-3 (b) and Figure 3-3(a) respectively). A reverse trend from 4 to 1 would be used for angles from 90 to 180 degrees. This allows for the number of counts to be consistent throughout the rotation without overexposing the sample. It must be noted that 180 degrees of

rotation suffice for such flat samples since the rotation from 180 to 360 degrees only provide redundant information of that of 0 to 180. Alternatively, a strip with a width of 1mm of the sample can be cut allowing the x-ray path length to be almost the same during the tomography. (Figure 3-3 (c)) It was observed that both remedies can contribute to the quality of imaging however cutting a strip of the sample can also enhance the transmission and therefore increasing the resolution in addition to signal to noise ratio enhancement offered by increase in X-ray counts. A probable issue with cutting a strip is the possibility of warping during thermal cycling which was observed no to be the case for the studied samples. In addition thin strip samples may be dominated by edge effects, which is the reason to select thicker samples for tomography in the next section.

3.1.3 Use of Energy Filter to Enhance Transmission

The quality of a 3D image is largely determined by the transmission value which is the percentage of the X-ray counts that passed through the sample and reached the detector. To obtain the transmission value at each point on a projection image, the image of the sample is divided by an image of air. Figure 3 shows how transmission values are obtained. The optimum value of transmission is believed to be 23-35% percent in the region of interest.

Figure 4 provides statistical information of the percent of transmission before and after using filter. Primarily the mean value of transmission in the shown region is less than 10 percent, we are therefore required to use an aggressive high-energy pass filtering which removes the low energy rays allowing high energy ones to go through. This obviously results in a reduction in X-ray counts but can contribute to increase in the transmission value. Figure 4 shows how the use of filter results in improved transmission values. More than 50 % increase in transmission is

achieved by using the filter but consequently the exposure time was needed to be increased by 50% as well to rectify the issue of reduced number of counts.

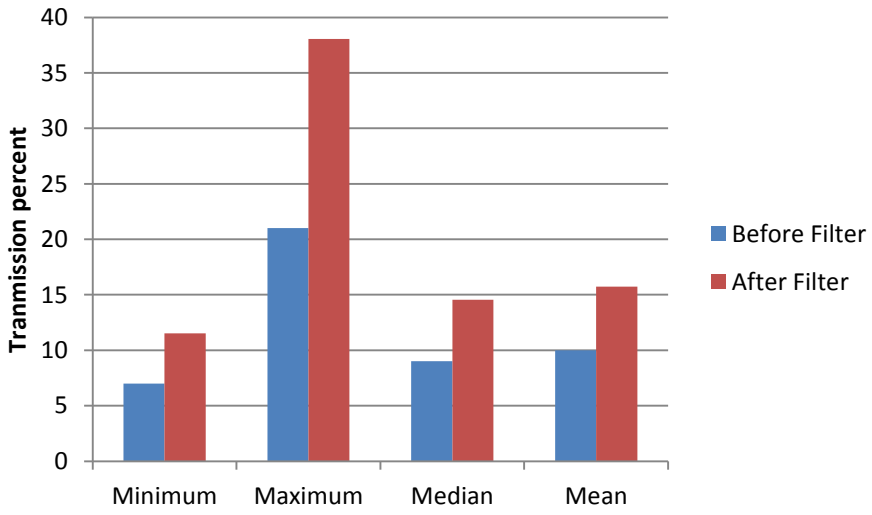

Figure 3-4 – Transmission percent with and without filter

3.1.3 Optimizing number of Projections

Increased numbers of projections can enhance the quality of imaging as smaller angular increments are used lowering the chance to miss a feature during tomography. On the other hand, an unnecessarily large number of projections results in longer tomography runs which can entail more movement and sample drift as mentioned earlier. In addition, it results in larger data file which makes it more computationally expensive for post-processing and image analysis. Therefore knowing the optimum number of projections is critical. In order to optimize the number of projections for imaging TBCs, the imaging was performed with 4000 projections having an angular increment of 0.045 degrees. However, 4 sets of reconstruction were performed. The first reconstruction was performed on the entire projections while in next trials only, 2000, 1000 and 500 images were chosen for reconstruction using every 2 and 4 images of the total 4000 projections. We then looked for discrepancy among the 3D reconstructed images. Figure 5 shows a series of 2D slices of the exact same locations using 1000, 2000 and 4000

projections. The contrast and brightness has also been optimized making sure that the change in quality is not the results of contrast manipulation.

By investigating images on Figure 3-5 and similar ones where the ceramic topcoat is chosen as the region of interest, one can see a remarkable improvement in quality and the ability to retrieve cracks are enhanced by increasing the number of projections to 4000 images. Similar procedure has been adopted for Figure 3-6. However, here the region of interest is chosen to be the borders between layers. This region is of particular interest for extracting surface geometry of bond-coat or the topcoat and also measurement of the thickness of thermally grown oxide. Bond coat material integrity is another area of interest to be assessed in images in Figure 3-6.

We can observe that Surface of the top coat can be analyzed with as low as 1000 image, however the interface geometry and thickness of the bond coat requires at least 2000 images to be retrieved. On the other hand, when it comes to material integrity in the bond coat and identifying different phases within the bond coat, the tomography has to have at least 4000 projections. Videos of all slices are also studies and similar quality issues dependent on the number of X-ray projections were observed. It must be noted previous tomography efforts on TBC were performed with 1005 projections[10] which, as it has been shown, entails some feature loss. Same process was performed for the images after the thermal cycling and 2000 projection was observed to be still sufficient.

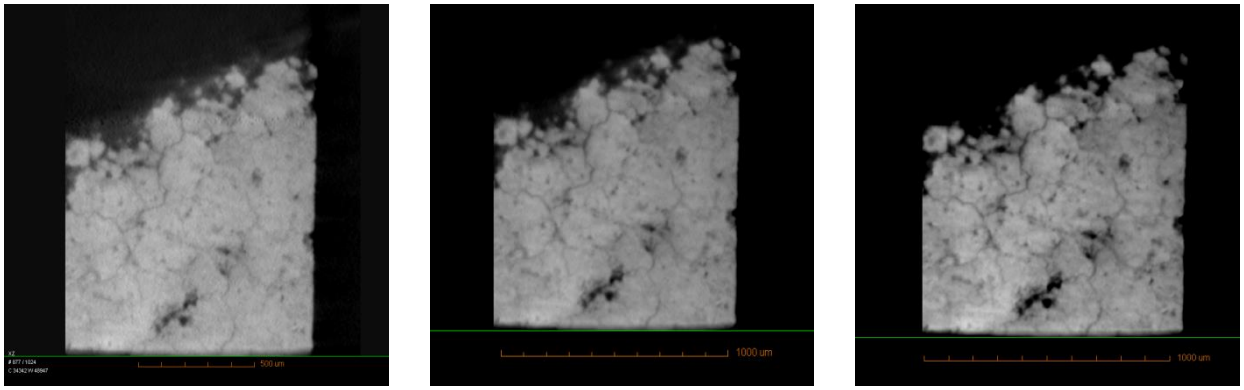

1000 Projections 2000 Projections 4000 Projections

Figure 3-5-Effect of Number of Projections on the quality of imaging TBCs- Region of Interest: Cracks in TBC

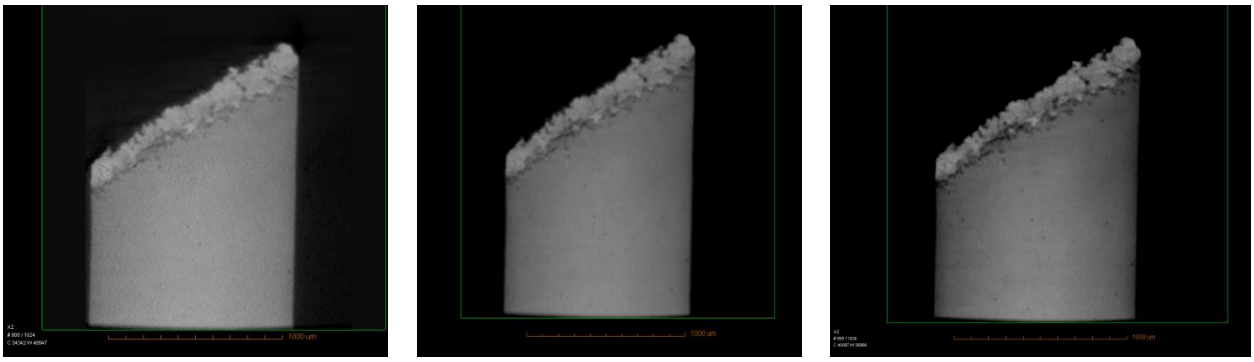

1000 projections 2000 projections 4000 projections

Figure 3-6-Effect of the number of projections on the quality of images- Region of interest: Borders of layers

3.2 Image Reconstruction

After acquiring projections, the 3D image can be obtained by 3D reconstructions of the X-ray projection. The automatic reconstruction results in poor quality of images and therefore reconstructions have been done manually using XMReconstructer software. (Zeiss, Flurton, CA) The main control parameters for reconstruction process are image center shift, beam hardening

and the kernel size of pre-reconstruction smoothing filter that will be addressed in detail as follows.

Center shift is the amount in pixels that the axis of rotation is offset from the center column of the detector. The effect of center shift on one reconstructed slice can be seen in figure 3-7 where a correct value of center shift results in more clear and focused images while image artifacts especially around the edges are present in images with wrong value of center shift. Beam hardening is the result of change in spectral characteristic as the X-rays pass through the sample, where the sample density remains the same but the light changes resulting in one area to be darker than another due to differential absorption with thickness that is also not spectrally neutral since low energy x-rays are attenuated the most rapidly. Also wrong beam hardening coefficient value may result in haziness on the edges of the sample.

Too Negative Center shift | Too positive center shift | Correct value of center shift

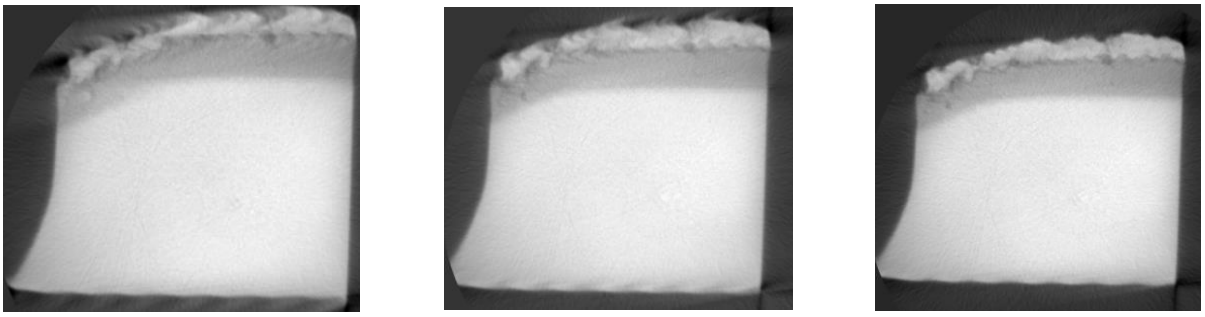

Figure 3-7-Center Shift Effect on Image Quality

A) Optimum value B) Optimum value C) Too large vale

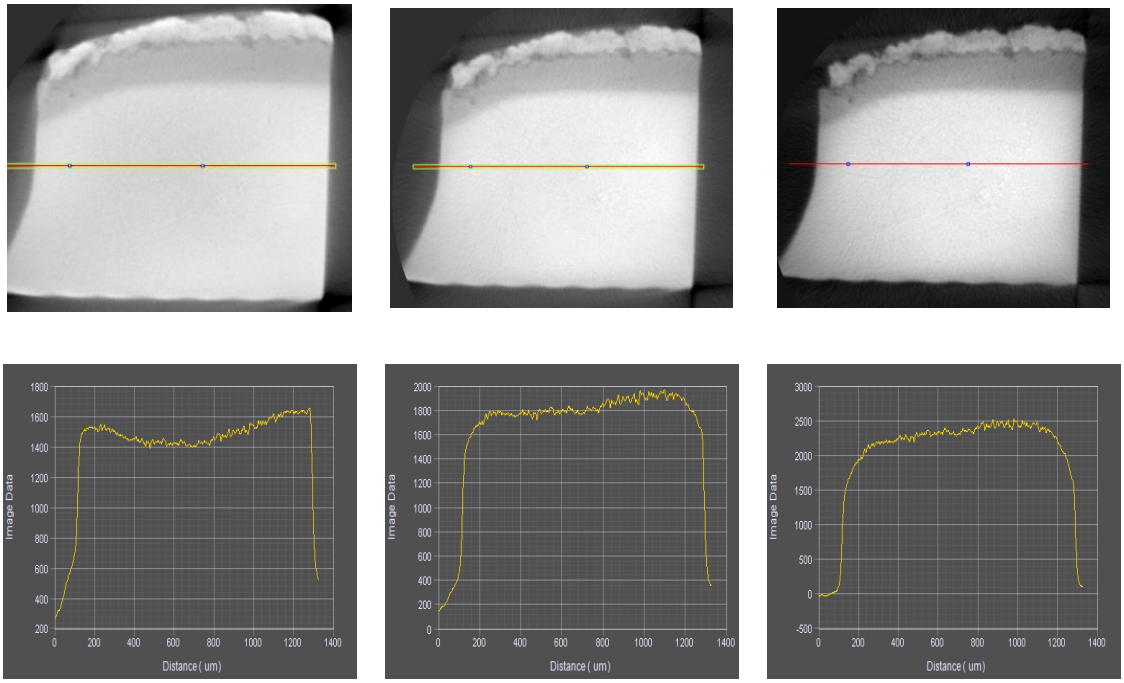

Figure 3-8- Optimization for beam hardening value

Figure 3-8 shows the correct beam hardening coefficient results in a more flat plot of the intensity versus position. It must be noted for choosing beam hardening the histogram is more important than the perception of human eye. As one can see the image (C) in figure 8 looks to have better contrast to human eye but the histogram which will be used for image segmentation lacks the quality seen in image (B).

Center shift and beam hardening values change for every tomography which makes it necessary to perform a repeatability check on data obtained after reconstruction.

Use of a pre-reconstruction smoothing filter involves a trade-off between resolution and signal to noise ratio. For the TBC samples of this study it was observed that post processing of the images will be greatly facilitated by higher kernel size values for smoothing. However it can also result

in loss of small features or compositional contrasts that could be observed using smaller kernel size. Therefore depending on the region of interest in the TBC, we used different kernel size. That is, if one is interested in the surface geometry of the layers, e.g. bond coat and the top coat, a larger kernel size can enhance the integrity for surface extraction during segmentation process that are discussed in the following chapters. On the other hand if we are interested in the cracks and voids in the TBC or the non-homogeneity in the bond coat and/or the super alloy composition, we need to use smaller kernel size. Figure 3-9 shows a reconstructed slice of exact same region from the same projection but with two different kernel size values.

Reconstruction Filter Kernel size=0.5 (minimum)

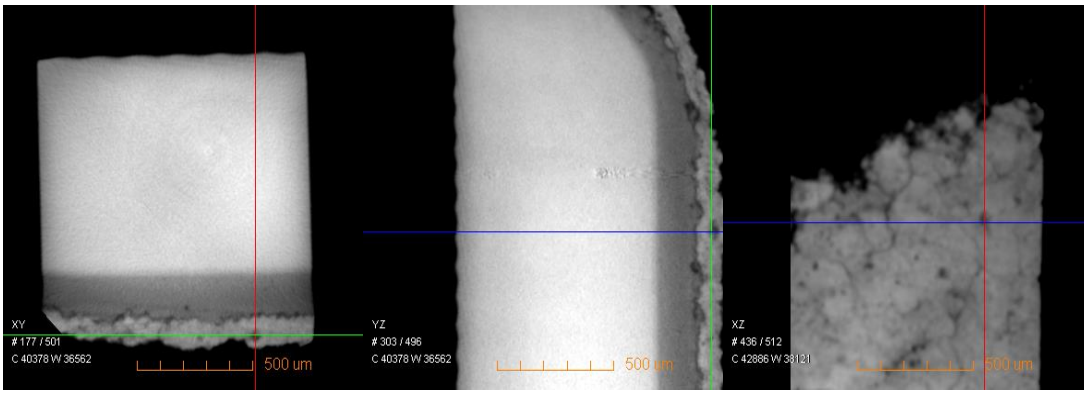

Pre-Reconstruction filter kernel size=1.4 (maximum)

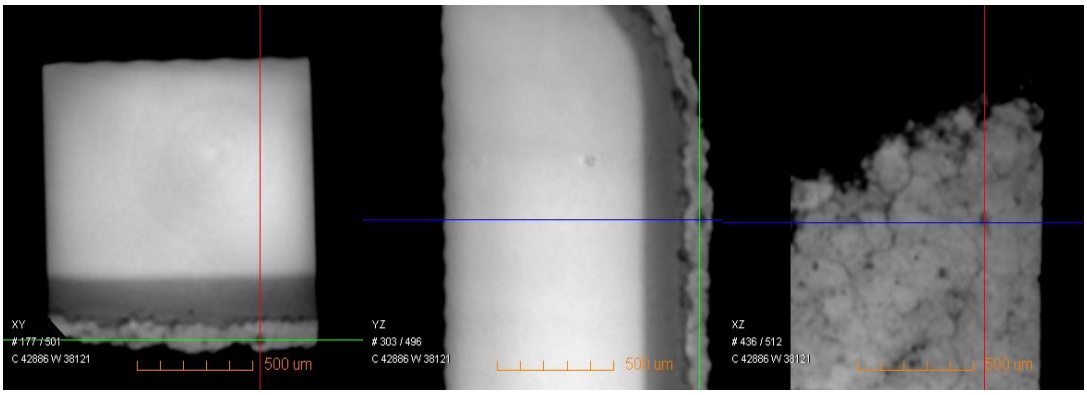

Figure 3-9-Effect of smoothing filter on image quality

Images with more aggressive smoothing lose the contrast on material composition difference inside the bond coat; some voids and cracks are also lost in the TBC but segmentation of the images is easier after aggressive smoothing. On the other hand the low values of smoothing are noisier but less blurry and less feature loss with more difficult segmentation process.

3.3. Image processing

After the reconstruction the images are imported to the post processing software, Avizo. (Visualization group Inc., Burlington, MA). In order to be able to perform any quantified analyses on the obtained 3D data, two major steps has to be performed.

1- Image segmentation (Assigning a specific material to each pixcel such as void, ceramic bondcoat …) and labeling: Assigning material to the pixels for quantified analysis.

2- Image Analysis: extracting quantified information from the segmented and labeled images.

3.3.1 Image Segmentation

Images need to be segmented and labeled for possible further quantitative analysis, that is different parts of the image has to be assigned to a different material. Even after filtering, some slices could not be automatically segmented. The authors therefore have used the magic wand option, offered by the Avizo software where certain regions can be selected manually slice by slice for the 3D image. This results in the most accurate segmentation especially for bond coat surface geometry. Figure 3-10 shows the result of the segmented image in addition to the extracted bond coat and top coat surface geometry. Following the segmentation, the images can be analyzed for quantified information. In the following sections of this work, different quantitative analyses of TBC are discussed.

a)

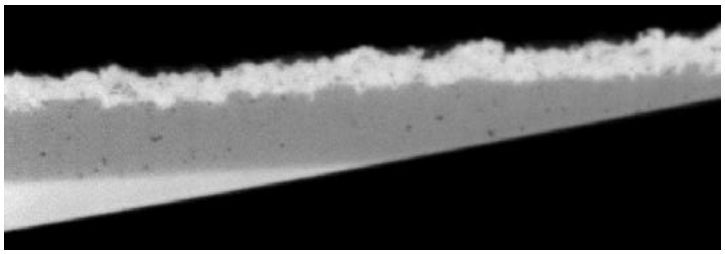

b)

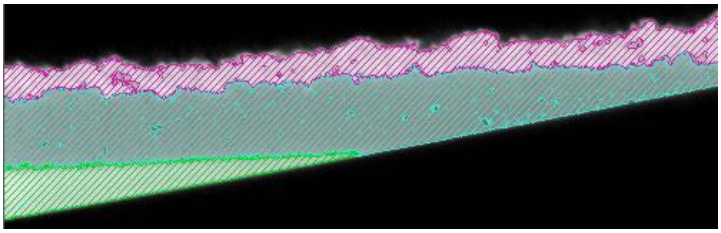

c)

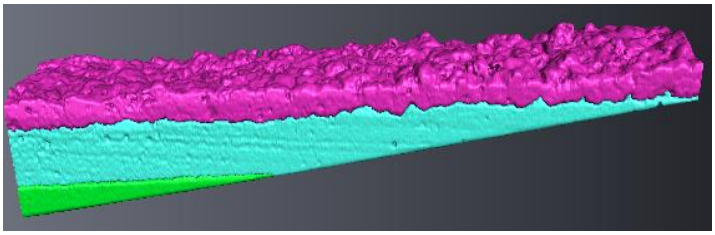

Figure 3-10-a)Image taken from X-ray, b) segmented image, c) 3D surface generated

3.3.2 Quantitative analyses of TBC layers and repeatability verification

As mentioned earlier one of the contributing factors to the failure of TBCs is the surface geometry change of the interface. CT scan is an enabling technology for characterization of surface geometry change of the bondcoat also known as rumpling. However, in order to quantify rumpling, one has to make sure that the method is repeatable enough to be able to distinguish between the real surface change and possible variations in surface parameters due to noise and errors due to lack of reproducibility of the results.

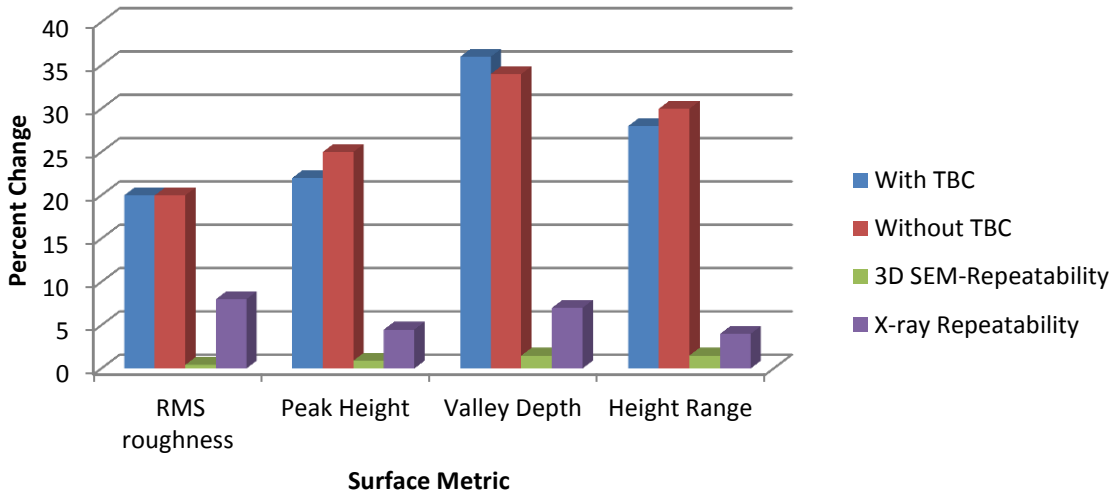

Figure 3-11- Repeatability analysis of bond coat surface parameters before and after thermal cycling with X-ray CT compared with stereo photogrammetry

In order to verify the repeatability of the proposed X-ray tomography technique, we have tried to image the same area of a sample repeatedly and extracted surface metrics already introduced by other 3D imaging as reported in [36] for quantifying rumpling on bare bond coat samples. Special precautions are also adopted to make sure that the same areas on the surfaces are being imaged and compared. Figure 3-11 shows the variation in each surface parameter during multiple X-ray tomography scans. The definition of surface parameters and their digital implementation can be found in previous works of authors and surface characterization references.

Comparing the variations with the surface geometry changes seen one can see that the increase in surface parameters due to rumpling are at least an order of magnitude larger than the observed variations of multiple imaging of the same area of the sample which has not undergone any thermal cycling. This proves that the X-ray tomography has the can be used for 3D

characterization of rumpling under the top coat non-destructively which cannot perform by any other imaging technique before.

3.3.3 Detecting Pores from Cracks

It was found out that the reconstructed cracks after segmentation are thicker comparing to the 2D virtual slices of the TBC. This problem is due to the 3D reconstruction algorithm of X-ray projections that utilizes Fourier transform. Since, the images are actually made from 2D projection, which are used to generate 3D images using Fourier transforms. From these reconstructed images one can extract man 2D slices referred to by Xradia as TXM files. On these images pixel thresholds are chosen to separate voids and cracks from TBC material. It was observed that at the edge of cracks and voids that we not as dark as the true crack presumably because the edge pixels include fractionally void and material. Labeling these edge pixels as void leads to apparent thickening of the crack images to make them look like voids in many cases. To correct this threshold for declaring a pixel to be a void was set darker level eliminating the identification of the edge areas as void materials. So doing the cracks was restored to realistic thicknesses. So we have limited the threshold range to make sure we are segmenting a crack and not the material. To also make sure that the cracks and pores are properly detected during the segmentation we have double checked them after segmentation visually on all slices of each sample. It should be noted that without this step cracks and voids could not be distinguished and nearly all important results concerning cracks could not be obtained.

3.4 Optimized X-ray Tomography Technique

Micro-CT is a suitable technique for nondestructive evaluation of internal structures of materials system. However, there are several parameters that need to be optimized before a high quality image can be acquired. In particular, for complex engineering structures such as Thermal Barrier Coatings with multi layers of highly X-ray attenuating materials such as Yttrium Stabilized

Zirconia (YSZ) and Super alloys of Nickel and Cobalt. We have classified the parameters that need to be optimized for a successful tomography into 3 main categories:

- *Sample Size:* It is important to choose the sample size such that sufficient X-rays can penetrate the sample and further collected by the detector. On the other hand, smaller samples can behave differently from realistic case. Therefore, sample size optimization is a significant primary prerequisite.

- *Image Acquisition Parameters:* Unlike common microscopy techniques such as SEM and optical microscopy when one can utilize an already well-established operating protocol, X-ray microscopy demands optimization of many imaging parameters without which the results cannot be used for analysis. These parameters vary from one type of sample to another and in sample types such as TBCs may even vary by region of interest.

- *Repeatability and Quantitative information:* Studying TBCs require imaging same location of a sample and trace evolution of asperities or cracks. This is not feasible unless robust image registration measures are adopted ensuring the exact same area is being studied at each imaging interval.

Following chapters will discuss the challenges in each of these three major areas and explain our proposed remedies to overcome them.

3.4.1 Optimizing Sample size

Compositional details of samples are presented previous chapter. We have also shown that samples at full size have failed after 220 to 250 hours of one-hour cycles at 1121 ºC. Figure 3-12 shows the sample and all the smaller ones prepared from such coupons. The existence of highly X-ray attenuating materials in these layers requires smaller sample preparation to allow more X-

rays to penetrate the sample. On the other hand, it is important to know how small of a sample is needed so that the sample behaves as closely as possible to the realistic conditions while the size of the sample don't impose any unwanted imaging artifacts. In preparation of such samples, there are two important criteria:

- According to the principles of micro-CT, it is desirable to have close to cylindrical samples, which helps having the same bulk of material in every angle as the sample stage rotates.

- It is also of interest to minimize the X-ray path length through samples by choosing the right mounting angle for the sample. For example, it is better to mount a rectangle sample vertically, rather than horizontally, where the X-ray path length is through the width of the sample. This particularly reduces an artifact in X-ray Microscopy known as " Beam Hardening" which can lead to a false contrast change within a material due to X-rays losing energy .

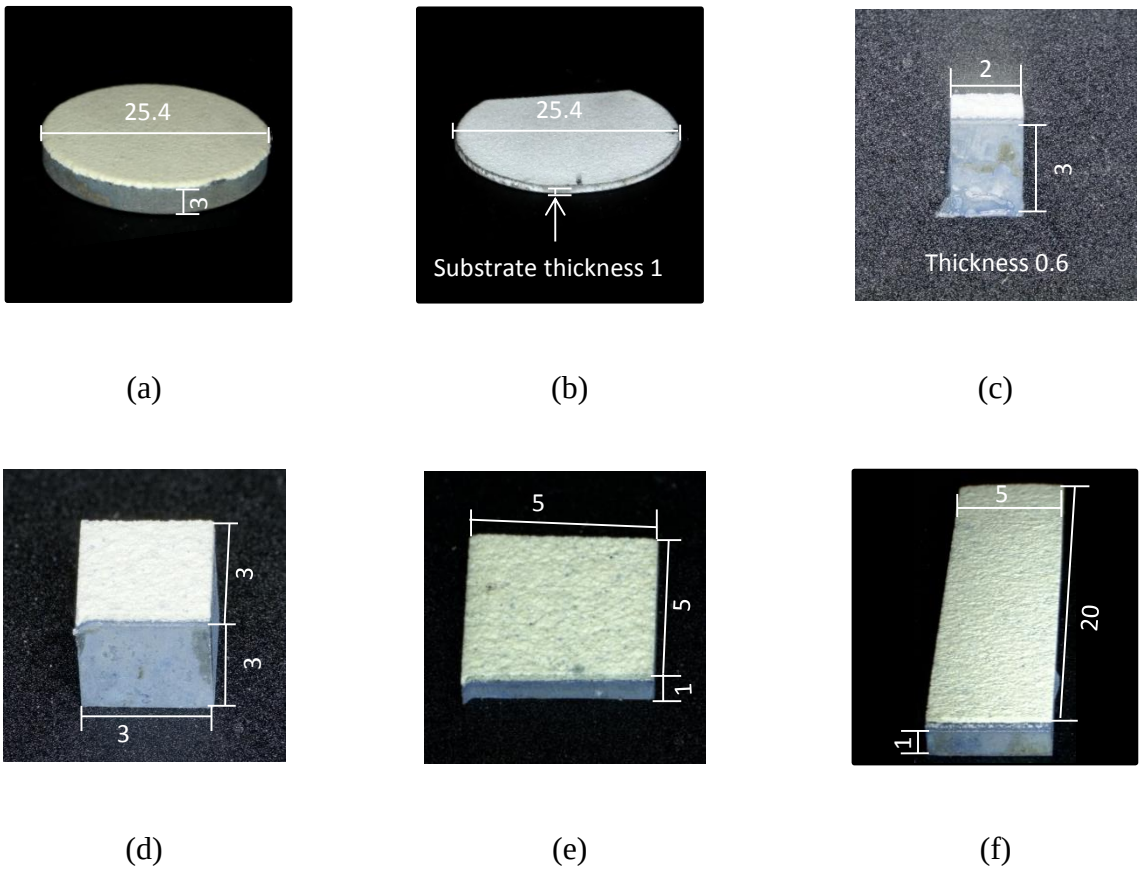

(a) (b) (c)

(d) (e) (f)

Figure 3-12– Six different sample sizes selected for experiments. (All dimensions in mm)

One way to create smaller samples is to leave all layers at full thickness but decrease the width of the sample. Samples (c) and (d) are examples of such remedy were the widths are 0.6 and 3mm respectively. This allows a much higher transmission of X-rays as they pass through the top coat. X-ray transmission rates through different thicknesses of the top coat can be seen in Table 3-1:

Table 3-1 – X-ray transmission rate for different path lengths

X-ray path length through top coat (mm)	**1**	**2**	**3**	**5**
Transmitted X-ray rate (%)	43	21	15	8

There is an inverse relation between the transmitted X-ray through a bulk of material versus the material thickness. We also found that the features in the top coat such as cracks and voids cannot be well recognized after reconstruction when the transmission values are less than 15 percent which is why the largest sample of this kind sample (d) has the width of 3mm.

Another way to prepare samples suitable for tomography is thinning down the substrate to 1mm while keeping the disk at its full diameter. (Figure 3-12(b)) Such samples should be then mounted vertically. The X-ray path length in this case is still very large at some angles during the rotation of the sample for tomography lowering down the X-ray transmission rate. To overcome this issue width of the sample is reduced to 5 mm (samples (e) and (f)). Such samples can then be mounted from their edges facing the source and X-rays will pass through all three layers during the tomography. Thanks to smaller thicknesses, the X-ray transmission rate reaches an average value of 22 percent which is sufficient for a reliable reconstruction. It must be noted that X-rays pass through all 3 layers resulting in much greater "hardening" of beams. Multiple samples (at least three) of each type b, c, d, e, and f were thermally cycled up to failure at 1121 ^{o}C, and 1 hour cycles. Table 3-2 shows the effect of sample size on the life of sample.

Table 3-2– Effect of size on sample's life

Sample name	**a**	**b**	**c**	**d**	**e**	**f**
Failure at 1121 ^{o}C (1 hr cycles)	220-250	220-230	180-200	210-220	220-250	210-230

And Figure 3-13 shows a single 2D virtual slice of 3D reconstructed image of each sample. Please note that in the thin full coupon case type (b), the thickness of the top coat is also reduced to 150 microns to obtain sufficient transmission.

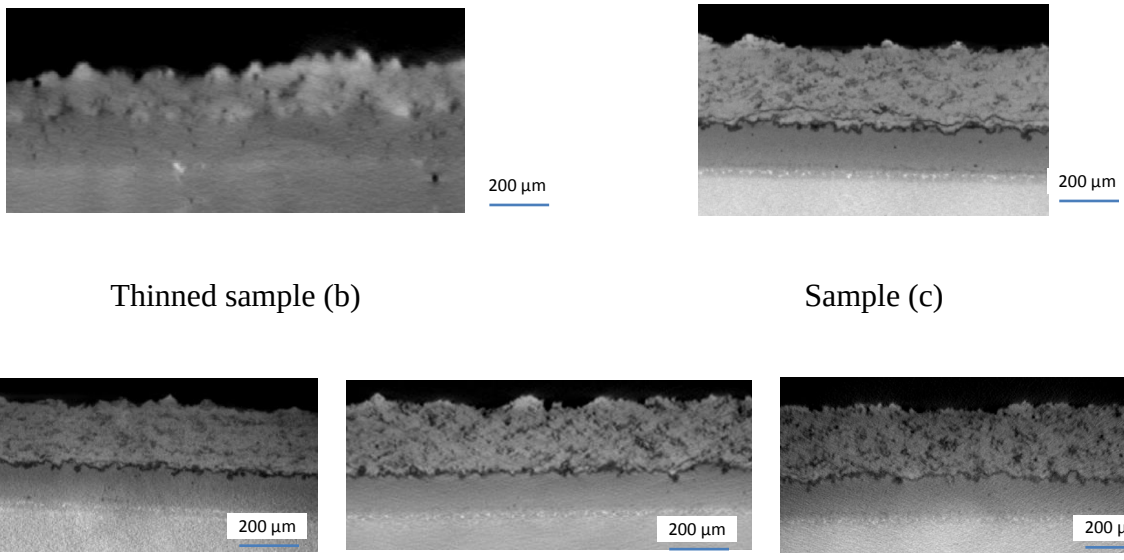

Figure 3-13— Virtual slice of reconstructed images for samples of figure 1 (all samples are shown after 25 hours of thermal cycling at 1121 C)

Combining the information in Table 3-2 and observation of figure 3-13, one can conclude a better quality of imaging is achieved when samples are smaller as in sample type (C), a 1 by 2 mm sample,. The images are less grainy and there is a better contrast between within the TBC. However type (C) sampled also fail considerably sooner than the full coupon. We can also notice the cracks are appeared much sooner in this type of samples. The authors attribute this to a known phenomenon in thermal barrier coatings commonly phrased as the "edge effect" [38] where edges of the samples undergo larger damage. Also, sample type (b) provides barely sufficient quality for studying the behavior of interfacial surface but lacks the resolution to retrieve cracks and voids. Samples (d), (e) and (f) behave very similarly to the full coupon at a

cost of slightly lower resolution which will further demand image processing for a better analysis. It must be noted for samples (d), (e) and (f) the time of tomography is also considerably longer which will be discussed in the following section. The smallest sample that gave similar lives to the full sized sample was sample type (d) which was 3mmX3mm and this offeres the shortest run time and best image quality of the samples that were large enough to have lives similar to the full sized sample. Therefor this is the preferred sample to be used for most of l the subsequently shown results with some results from the 5mmX5mm samples as well.

3.4.2 Optimizing Image acquisition Parameters

In this study, we have used Zeiss Xradia versa 510 X-ray microscope at its maximum voltage and power of 160 (Kv) and 10 (W) to have sufficient transmission for TBC samples. The real picture and architecture of the system can be seen in Figure 3-14 (a) and (b). As opposed to medical CT scanners, here the source and detector remain stationary during tomography, while sample rotates at user-defined increments to create a stack of X-ray projections. As one can imagine, there are many parameters that can affect the quality of images including:

- Distance of source and detector from the sample
- Number of X-ray projections
- Detector Magnification
- Exposure Time

These parameters can affect the pixel size and signal to noise ratio, which need to be optimized based on region of interest.

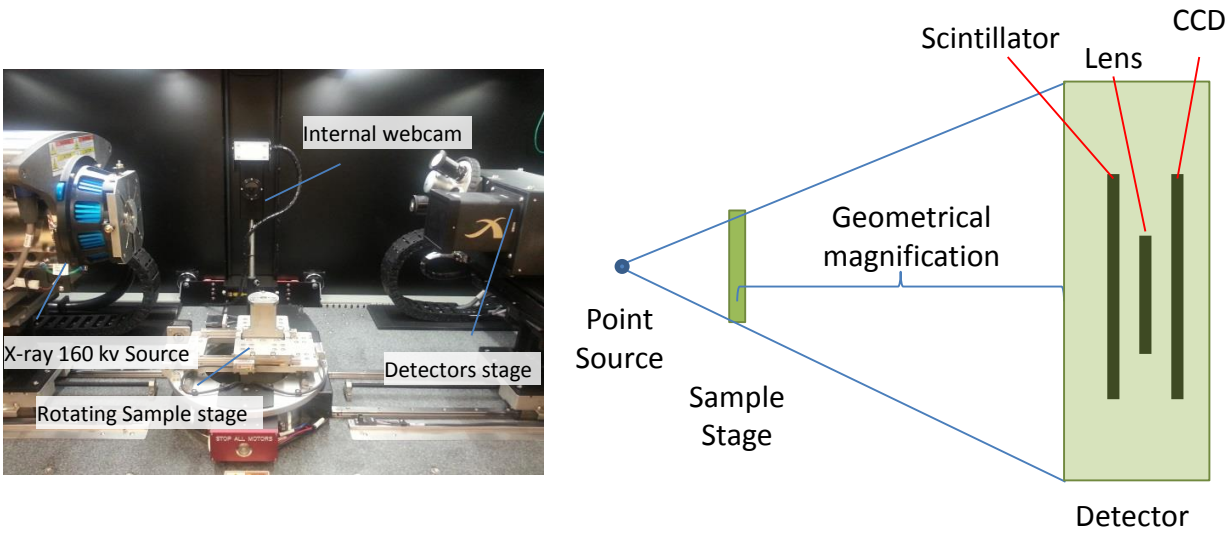

(a) (b)

Figure 3-14- Zeiss Versa 510 inside view

3.4.3 Optimizing the pixel size and X-ray counts: Trade-off with tomography time

One critical parameter that can define the quality of 3D reconstructed images is the pixel size based on which many other parameters such as Distance of source and detector from the sample (geometric magnification) and Detector Objective (similar to optical magnification) will be tuned. To use both magnifications effectively, one has to optimize them simultaneously. Thanks to a near-ideal point source used in the cited system, we are given the opportunity to move detector and source towards or away from one another while maintaining the resolution [39] and change the corresponding pixel size. Geometrical magnification can help to decrease pixel size by factor of 10 in addition to the magnification offered by the detector which is yet another option to be tuned. Combining the two magnification types, one can choose any value between 0.3 to 62 microns for the pixel size. Each detector in turn has specific number of pixels (about 1000) which can define the field of view for imaging. However there is a trade-off. Smaller pixel

size demands the detector to be positioned relatively far from the source thus reducing the number of X-ray counts detected by the detector. Based on the principles of wave propagation, wave power is inversely proportional to square of distance from wave source. The same concept applies here. The following diagram, Figure 3-15, shows the relation between the detector distance and X-ray counts as it moves back. The values for distance and X-ray counts are normalized based on the maximum value for each to better show the dependent behavior of these two parameters.

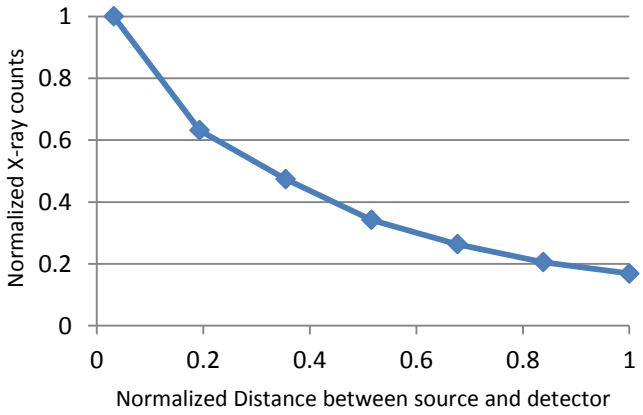

Figure 3-15- X-ray counts relation with respect to the distance between source and detector

In order to get a clear image, one has to obtain 2D projections with more than 5000 X-ray counts. In order to maintain such values, one has to increase the exposure time as smaller pixels sizes are needed resulting in longer scans. Table 3-3, shows how the total tomography time is affected by the selected pixel size and related exposure time.

Table 3-3- Total tomography time relation with respect to pixel size and exposure time

	Scan 1	Scan 2	Scan 3
Pixel size (µm)	4.95	2.99	1.49
Window size (µm)	4992	3020	1504
X-ray counts	6000	6000	6000
Detector distance (mm)	19	66	186
Exposure time (s)	1	3	12
Number of projections	1000	1000	1000
Total tomography time	37 min	1 h 12	3 h 50 min
Suitable for …… In TBCS	Qualitative studies	Surface Geometry study	Studying Crack Evolution/ TGO thickness

For studying thermal barrier coatings, depending on the region of interest, different values of pixel size are desired. We have seen that for qualitative analysis, pixel sizes in the range of 4-5 microns are sufficient. To perform quantitative analysis such as recording surface geometry, one has to have a pixel size of 2-3 microns and to be able to image larger areas. Smaller values (less than 2 micron) are used for imaging cracks, TGO thickness and voids in the top coat which result in even smaller fields of view. It is important to note that the pixel size is different from

detectability. For example, at pixel size of 1 micron, one can detect features of almost 50 nanometer in size. [40]

However, stitching can be an option that provides us with the opportunity to look at a larger field of view while maintaining fine resolution at the cost of increasing time and data size of the tomography. Stitching is to connect images from several areas with fine pixel size to generate an image with larger window size and same pixel size. Figure 3-16 shows how 3 smaller scans are stitched together to have the image a strip with the length of 6 mm at submicron resolution.

The important criteria to observe during imaging for stitching purposes is to let the images have at least 25 percentage of overlap for each area so that they can be detected during the post image processing and better stitch the images.

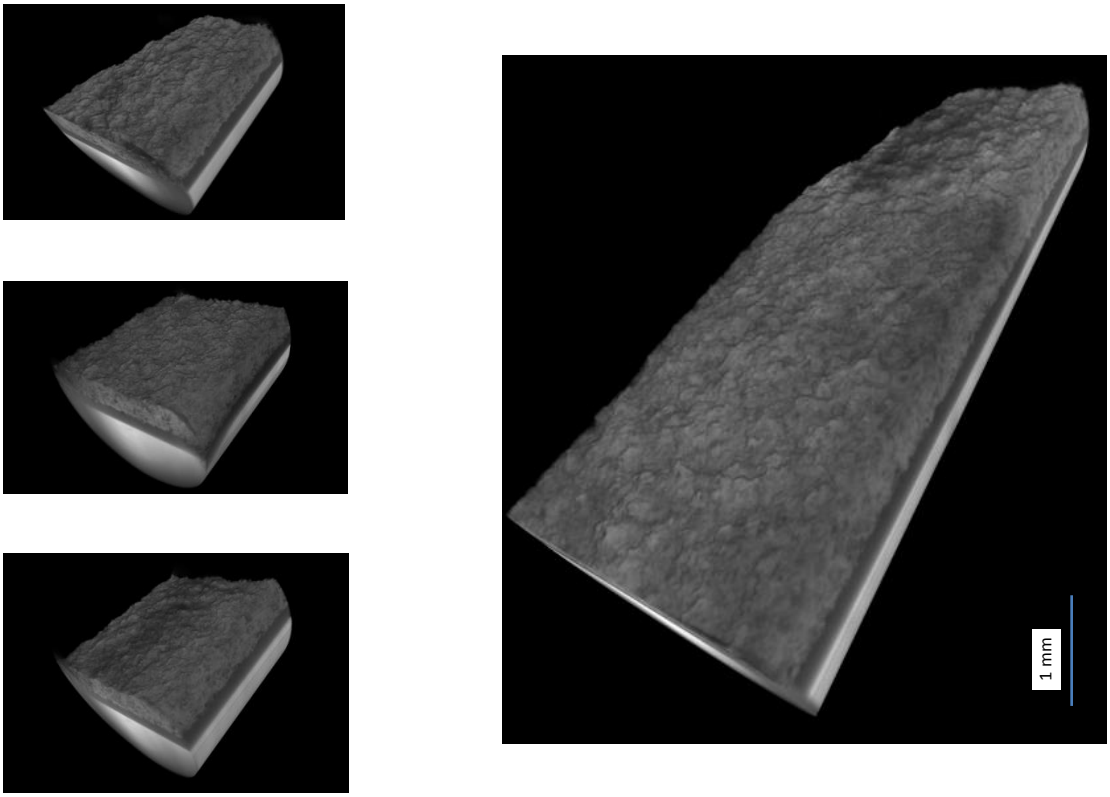

(a) (b)

Figure 3-16- Stitched image, 3D representation of smaller scans (a), and stitched (b)

3.4.4 Optimizing Repeatability: Image Registration

The ultimate goal of use of X-ray tomography in studying the TBCs, is study the evolution of individual asperities and cracks during heat treatment. It is, therefore, important to make sure that the exact same area is imaged after each interval of thermal cycling. We have used two registration techniques: one before imaging (pre-registration) and one after image acquisition (post-registration)

Pre-registration is done based on visual alignment of features and localization of the region of interest considering its distances with respect to the sample edges before tomography. Feature based pre-registration step has been done on two different angles of the two dimensional (2D)

projections. In the first step theX-ray tomography imaging field of view will be increased to the maximum level where the whole sample can be seen in the field of view. Centering the sample in the two directions of X and Y with respect to the window will approximately centralize the sample on the same area each time. In the next step the proper pixel size will be selected and the window size will be reduced where whole sample is no longer in window and the 2D projections of features are not too small to be detected visually. So one can recognize features before and after thermal cycling by rotating the sample in the same area. Thanks to the geometrical magnification, pixel size is set to be the same with the accuracy of 0.001 micron before and after thermal cycling for each tomography. The last step is to register the features visually to make sure the same area will be imaged as it is shown in Figure 3-17.

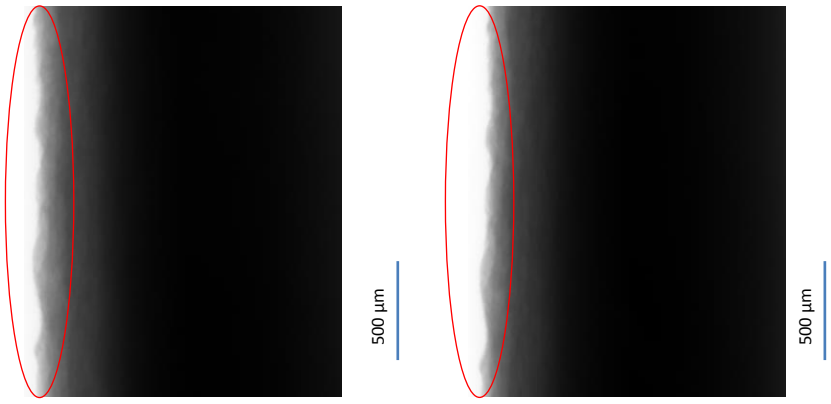

a) After 50 hr thermal cycling at 1121 ˚C

b) After 100 hr thermal cycling at 1121 ˚C

Figure 3-17- Pre-registration of 2D projections in 90 degrees

In addition to pre-registration process, post registration of the images has to be done after the reconstruction step. The reconstruction process will finally provide the 3D volume of the imaged

area, but it is very difficult to mount the sample with the same exact position with respect to source and detector every time. So there will be small rotations of the reconstructed image around different axes, which will result in seeing features of one plane before thermal cycling in several planes after thermal cycling. In order to find the same plane for both images, one requires changing the angle of the plane with respect to the related axes virtuallyso that same features will be shown in one slice as before thermal cycling shown in Figure 3-18.

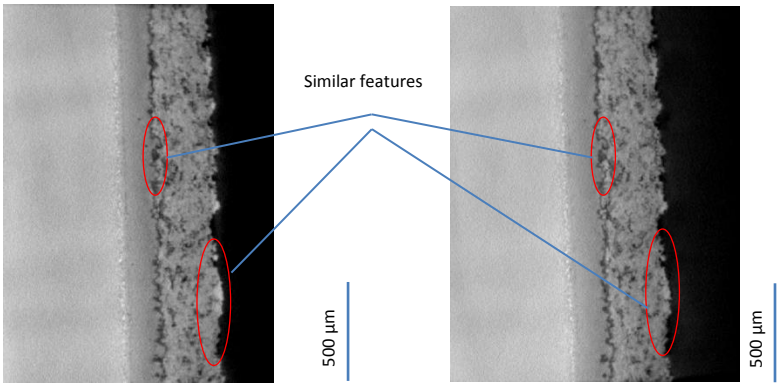

a) After 50 hr thermal cycling at 1121 ˚C

b) After 100 hr thermal cycling at 1121 ˚C

Figure 3-18 - post-registered reconstructed images

In order to check the repeatability of X-ray tomography, following our two-step registration procedure, an identical sample has been imaged twice. However, after the first imaging, the sample is taken out and mounted again for the second scan. Pre-registration process has been done on the sample to locate the same spot for imaging and then the tomography is performed. After doing the segmentation, which is to assign material to each layer of the sample based on the pixel contrast [41], 3D surface is generated, as it is shown in Figure 3-19, for both scans and surface parameters are calculated according to figure 3-19.

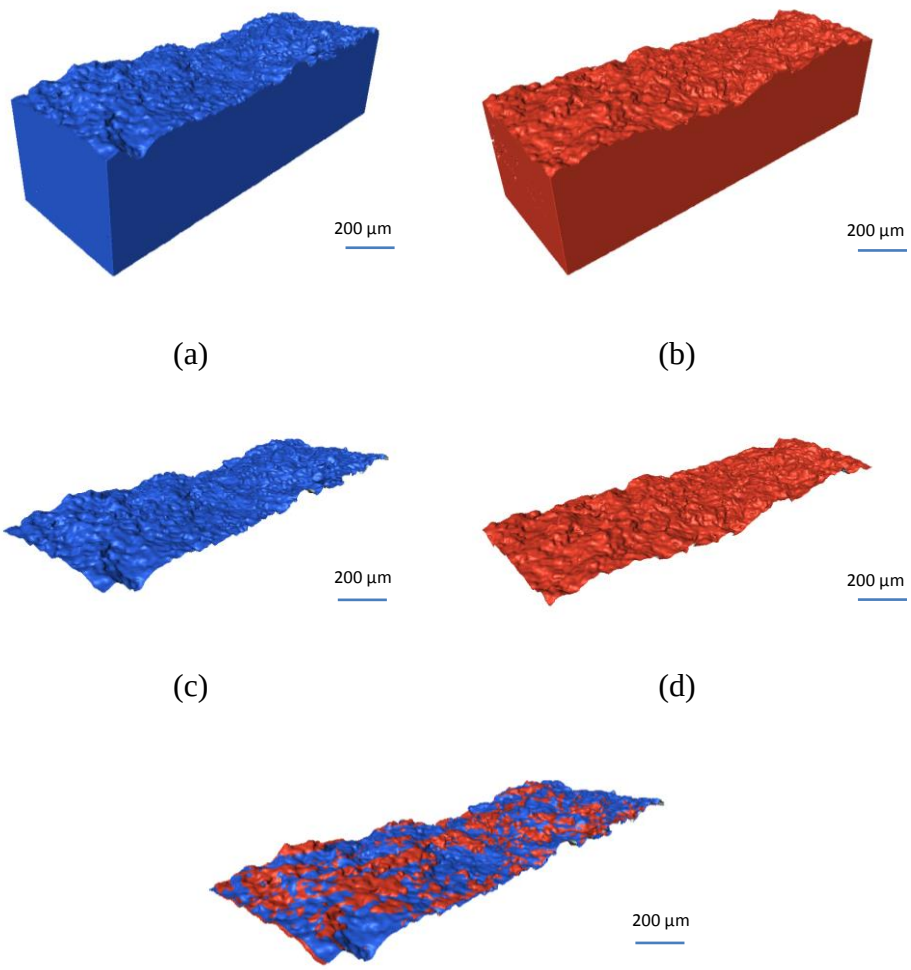

Surface height (µm)	First Scan	Second Scan	Error (%)
Average	73.56425	73.60109	0.0501
R.M.S.	73.68827	73.72794	0.0538
Maximum	124.47600	125.26200	0.6314

Figure 3-19-Repeatability check of the XCT, Surface generated for same sample in two scans in (a) and (b), top surface is separated from each scan (c) and (d), two surfaces are aligned (e)

It is seen that the Average, R.M.S. and Maximum values are very close to each other and the error is about 0.5 percent for the two sets of scan of the same sample twice, which defines the repeatability of this imaging technique.

3.5 Results

It has been shown above how to quantify the images information from X-ray tomography. These results are for a 100 micron thick APS TBC. Tortuosity analysis on the bond coat has been shown to be one of the effecting parameters in TBC failure [52].

a)

b)

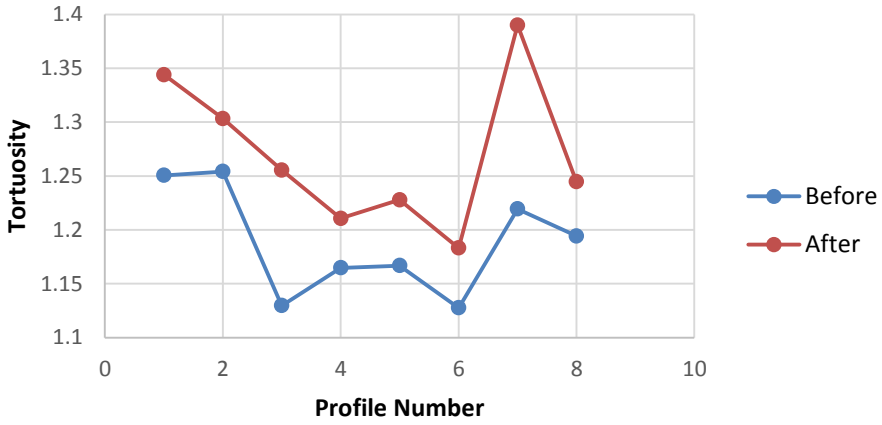

Figure 3-20- Line tortuosity change for a) bond coat and b) top coat using X-ray tomography

Although bond coat rumpling has been investigated widely but the top coat surface changes has not been studied as extensively. Since top coat is the free and accessible surface it is of great interest if the bond coat behavior could have been analyzed based on the top coat surface behavior.

For this reason both top coat and bond coat profiles tortuosity are calculated and compared before and after thermal cycling for selected profiles. There are 7 profiles selected from the generated surface with 40 micron distance in between which is the size of the surface characteristic wavelength [35]. This way of selecting the profiles minimizes the chance of the dependency between the profiles. Figure 2-20 shows the change of the tortuosity for the selected profiles both on top coat and bond coat before and after the thermal cycling. It is found out that tortuosity average for the all profiles is increasing from 1.16 to 1.26 for the bond coat and from 1.18 to 1.26 for the top coat. This simultaneous increase on both surfaces shows there is similar behavior for the two surfaces when sample is thermally cycled. Based on the difference of the changes in the tortuosity values for both surfaces it can be concluded that when the bond coat rumpling is increasing by about 8.5% then the top coat is increasing about 6.8% which is about 80% of the changes in bond coat. In other words, if the top coat tortuosity was recorded, the bond coat changes are about 125% of the changes recorded from top coat for this coating and probably for coatings of a similar thickness. This can introduce new non-destructive evaluation methods for failure prediction in thermal barrier coatings.

In order to further investigate the dependency of the two surfaces behavior correlation coefficient, which quantifies the dependency between two series of data or measurement, is also calculated for the profiles. Results are shown in figure 3-21 where the average of the correlation between the top coat and bond coat profiles before thermal cycling is about 91 percent which

becomes about 85 percent after thermal cycling. This shows that the dependency of surface behaviors is still considerable after thermal cycling.

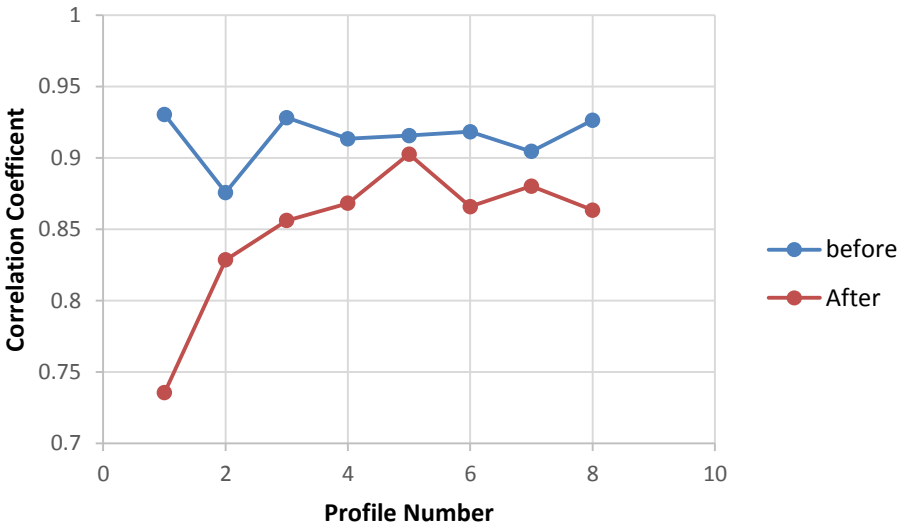

Figure 3-21- Correlation coefficient between top coat and bond coat profiles before and after thermal cycling

3.5.1 Interfacial Surface Geometry Change

One huge advantage of micro-CT is investigating the change in interfacial surface geometry under the topcoat nondestructively and through time. Figure 3-22 shows an example of such analysis where a common quantitative parameter for such studies known as tortuosity [42] is being measured before and after thermal cycling at only 20% of life.

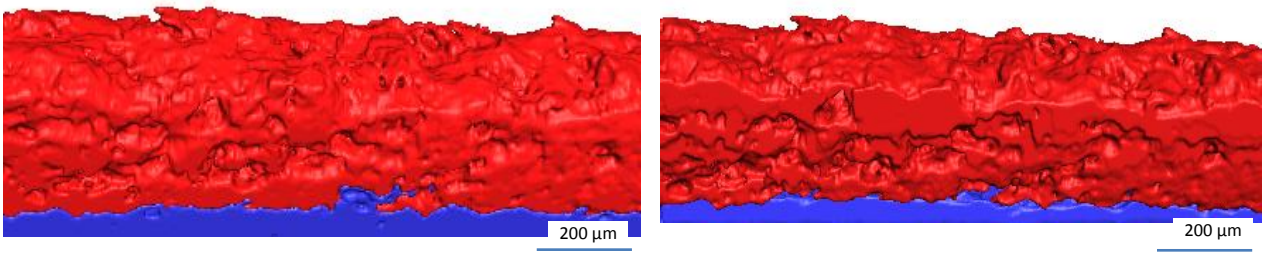

Before thermal cycling After 40 hr thermal cycling at 1121 ˚C

BC tortuosity Before :1.1584315 After : 1.1664286

Figure 3-22- Segmented TBC image

3.5.2 Crack evolution

The unique capability of micro-CT allows tracking the number of cracks and recording their evolution.

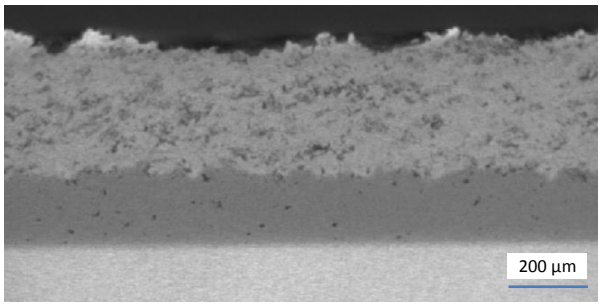

Before cycling

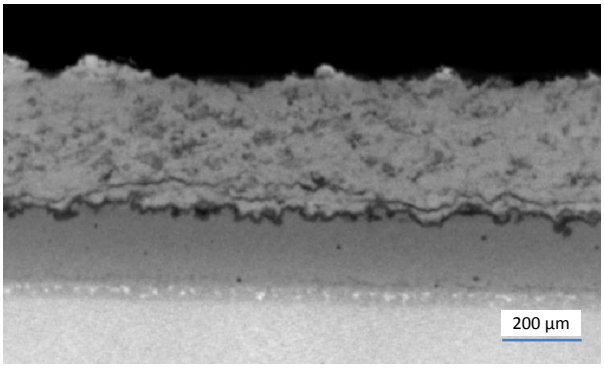

After 75 hr cycling at 1121 ˚C

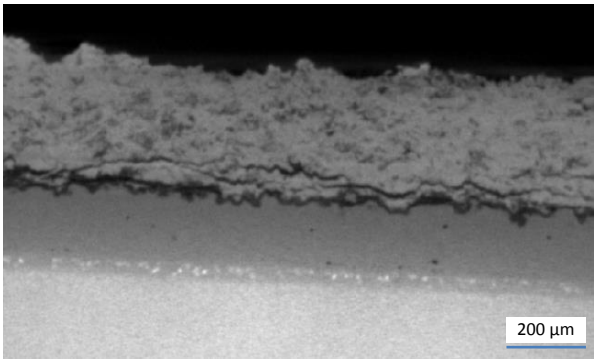

After 150 hr cycling at 1121 ˚C

Figure 3-23- Crack propagation tracking

	TGO thickness (µm)	Number of cracks	Crack length (µm)
Before cycling	0	0	0
After 75 hr cycling at 1121 ˚C	3.5-4	7	100-350
fter 150 hr cycling at 1121 ˚C	5.5-7	6	150-400

Figure 3-24- b) crack tracking parameters

Figure 3-23 and 3-24 provides an example of quantitative analysis that can be performed using micro-CT data. In addition, all the layers in addition to cracks can be rendered in 3D following appropriate image processing steps. Such an image opens up new analysis opportunities such as crack shape change, crack linking and position of cracks with respect to interfacial surface asperities which are discussed in later sections. Figure 3-25 shows how the cracks and voids are rendered in 3D inside the top coat.

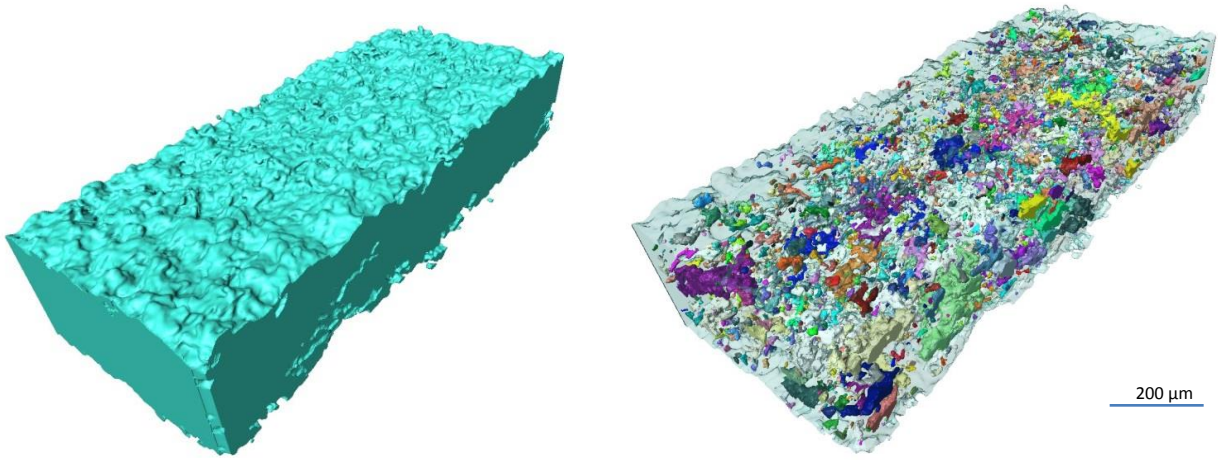

a) Top coat *b) Top coat internal pores and cracks structure*

Figure 3-25– Crack and pores observation in a segmented image

Chapter 4 Crack Analyses

4.1 Visualization of TBC internal structures

3D images of multiple samples, which were cycled till failure, are reconstructed for further analyses of each sample. Although the tomography is done on the same area every time after thermal cycling, it is a bit tricky as will be discussed in next section to find the same crack every time when the sample is mounted for tomography. In order to accomplish this, one has to consider the features in every slice during tomography, where the crack is present. Considering the fact that the window size is close to 2000 micro meter and the pixel size is selected to be 1.9 micron, the pixel size will be also the thickness value for each 2D virtual slice. These slices are in fact generating the 3D image. Seeking the similar features on these slices, where cracks are also present, for each round of cycling is the initial step to be able to compare the same cracks. In figure 4-1 these slices are presented for sample type c which is a 1 by 2 mm sample.

As it is seen in figure 4-1 the same cracks are imaged at different stages of the cycling process. Since the same area is imaged the process of choosing the cracks is possible and still tricky as follows. Starting from the latest scan images, which is the one before failure; one can go through the slices and find a specific crack. Same crack can be tracked back in previous scan's slices by considering both crack shape and the neighborhood features. This will give the opportunity to find the starting point of the crack and study possible reasons for the crack to grow in that specific region, such as surface parameters change, presence of pores in the neighborhood, and other possible ideas to study the conditions for crack initiation location. In the following, cracks are segmented and visualized using Avizo fire version 8.01 software and the observed behavior is explained in more details.

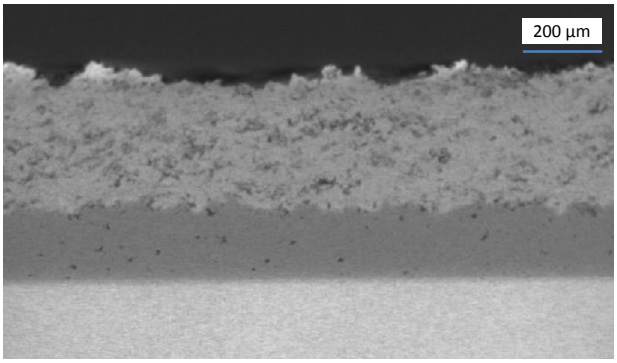

Before thermal cycling

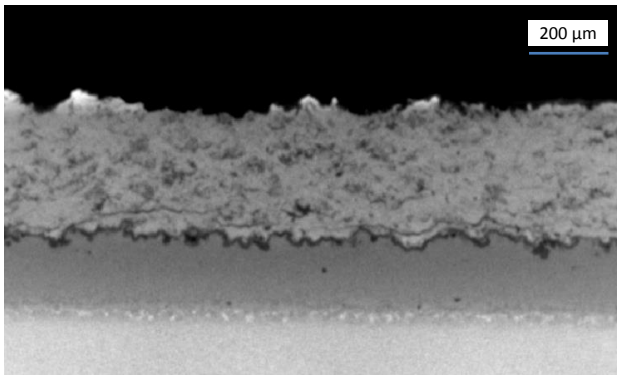

50 hour cycled at 1121˚C

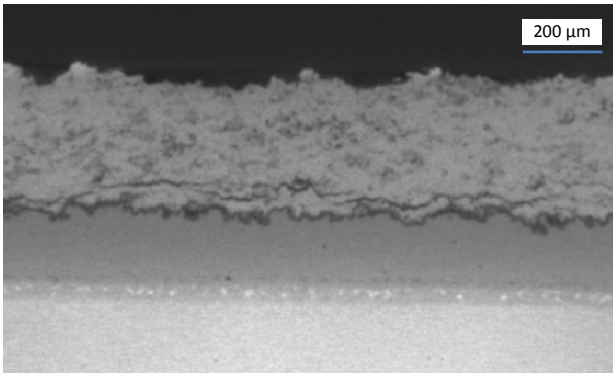

100 hour cycled at 1121˚C

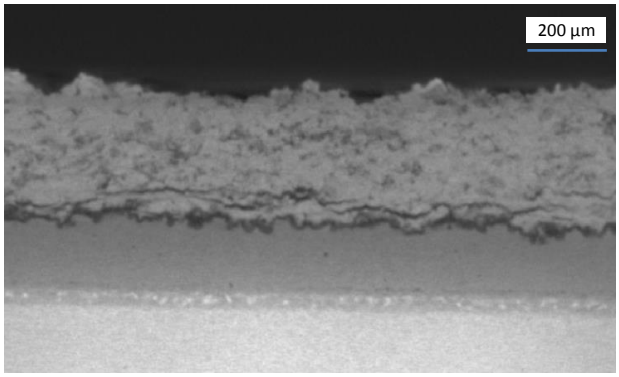

125 hour cycled at 1121˚C

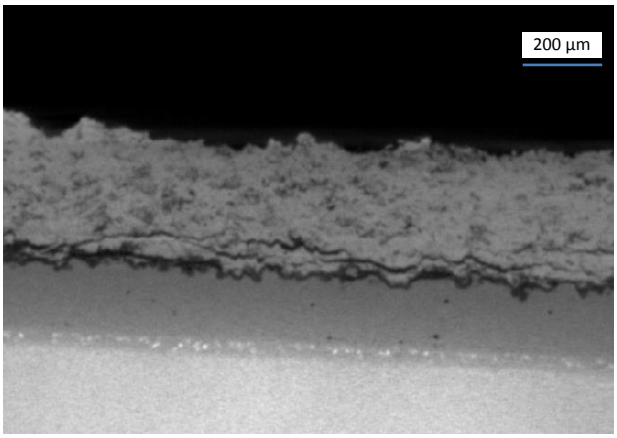

150 hour cycled at 1121˚C

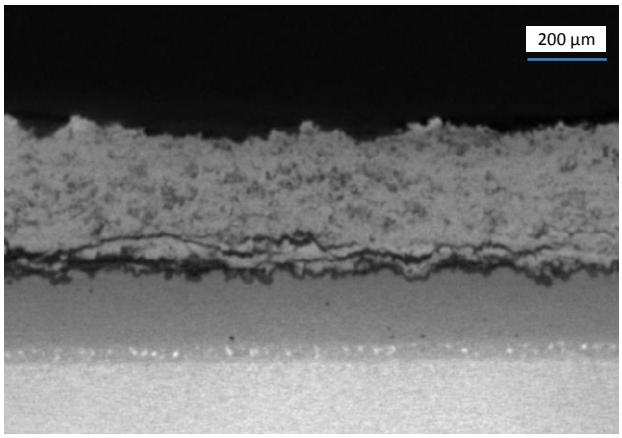

175 hour cycled at 1121˚C (failure)

Figure 4-1- A progression of X-ray tomography images of sample (a) from thermal cycling experiments

Thanks to the image processing software and supercomputers with high computation capabilities it is possible to segment the large size image files into, areas representing TBC, bond coat, and regions consisting of cracks voids for files of X-ray tomography in minutes. Taking benefits from the segmentation tool in Avizo software, which is to assign a material based on the pixel contrast; and using limited range brush tool, one can segment the exact area of cracks and visualize them separately in 3D. This was done for each of the scans separately and the crack shape and shape change during cycling will be well presented. In the following figure the cracks are presented for each cycled period separately.

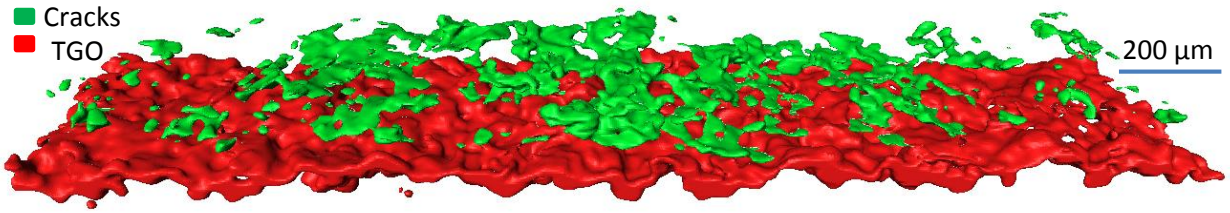

a) 50 hours thermal cycled at 1121 ˚C

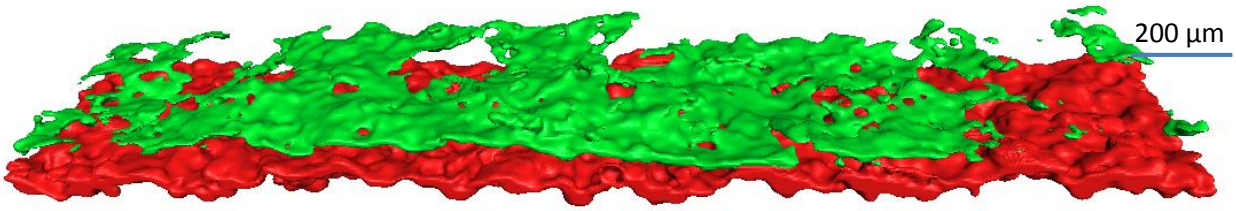

b) 100 hours thermal cycled at 1121 ˚C

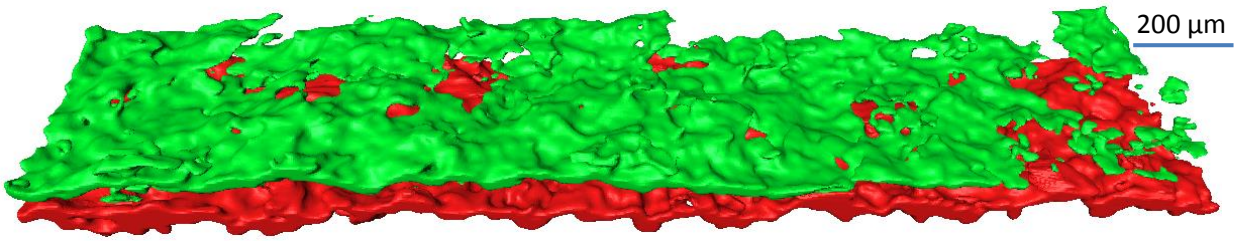

c) 150 hours thermal cycled at 1121 ˚C

Figure 4-2-Cracks and TGO presentation of sample (a) during multiple cycling

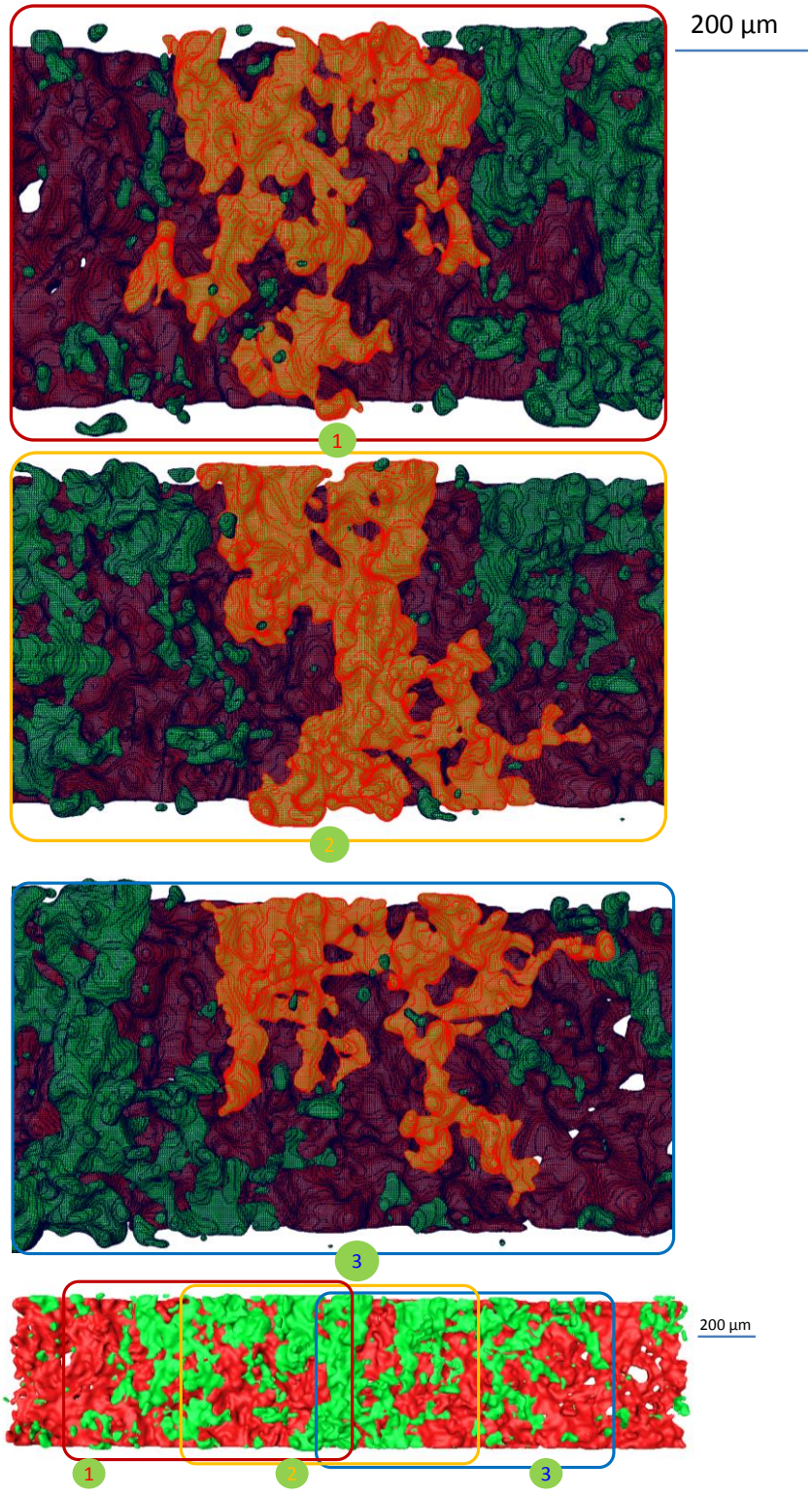

Figure 4-3– Separated cracks before linking in the 50 hour thermally cycled sample at 1121ºC

According to figure 4-3, which shows the three large cracks selected and shown separately from the original figure at the bottom, one can select cracks separately using the magic wand tool in surface editor and do any kind of analyses on it. It is seen in figure 4-3 that there are many small cracks but three large size cracks which are probably created by linking the smaller cracks and pores during the thermal cycling. But in figure 4-4 it can be clearly seen that those three large cracks are now linked after another 50 hour of cycling, which was also shown in figure 4-2 b, and have created one larger crack that can result in the failure of the TBC.

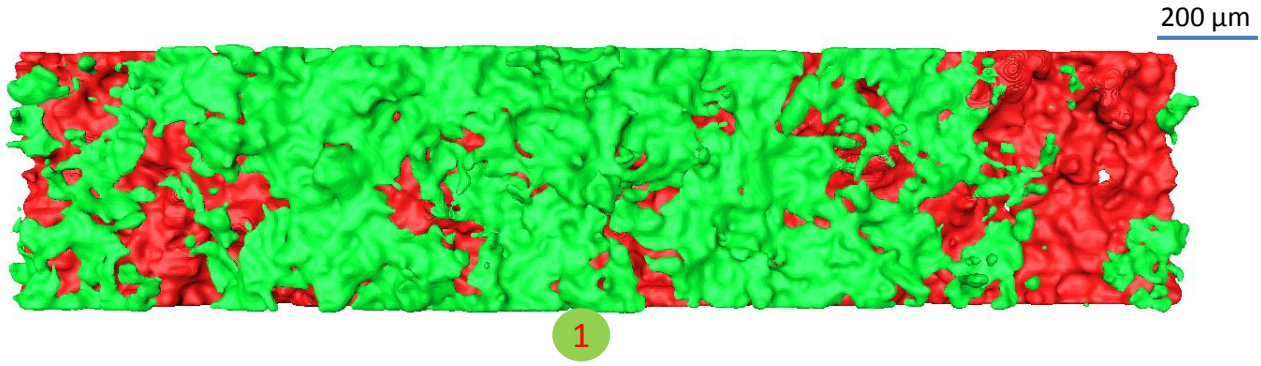

Figure 4-4– Cracks linked and selected as a single crack

As it is seen in both figures 4-3 and 4-4, crack shape and linking are well presented in 3D. In order to further investigate the conditions of crack linking many different cases are considered. In the following the same crack tracking process is performed on sample type (d) which is the 3 by 3 millimeter sample. In figure 4-5 (a) it is seen how the cracks are located with respect to bond coat asperities especially in their early stage. To further investigate the relation between the crack initiation location and bond coat surface parameters, the mean radius curvature of the TGO surface is calculated by fitting a cubic spline to the surface and then deriving the curvature information, Fig. 4-5 (b). It looks like cracks mostly tend to initiate over or around a summit.

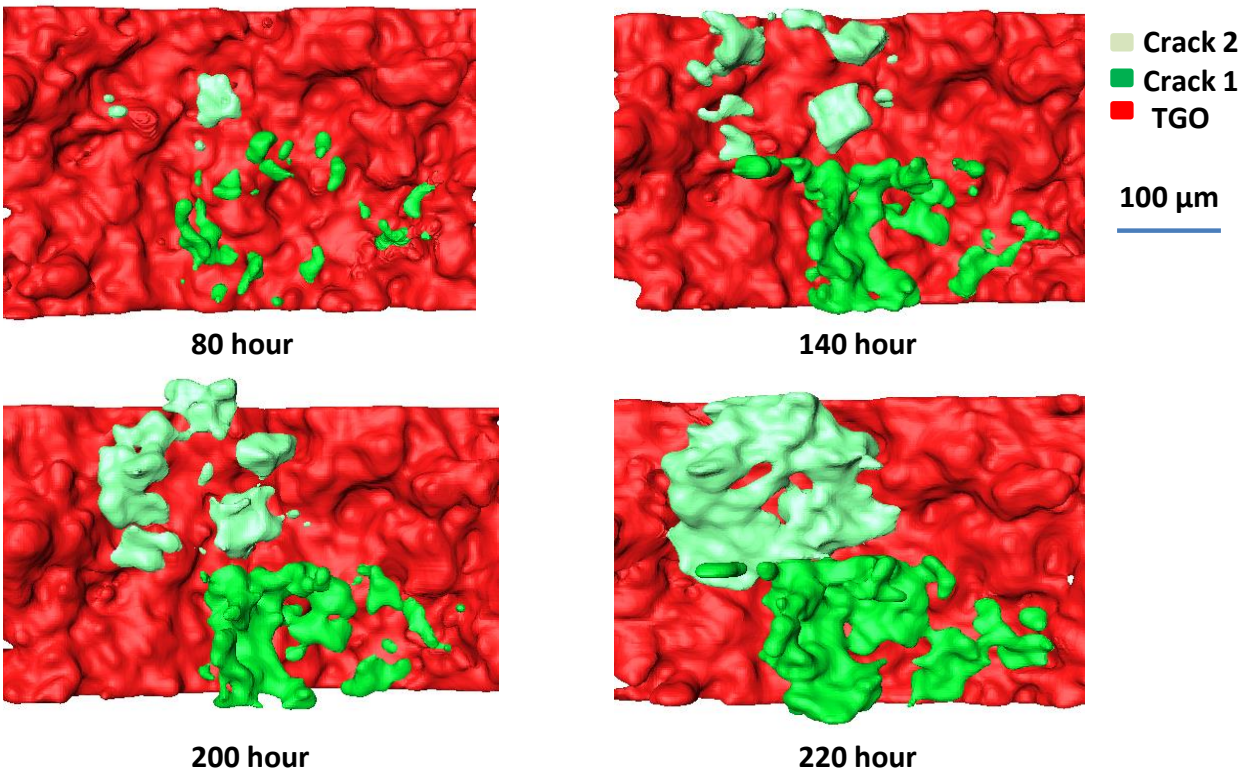

(a)

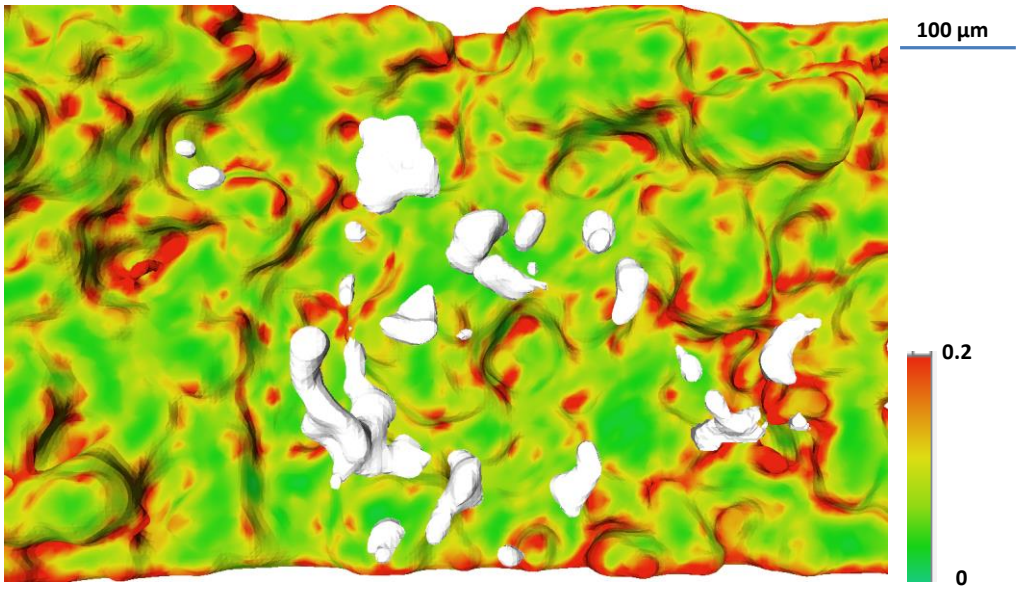

(b)

Figure 4-5 – a) Crack growth in a 3 by 3 size sample, b) Presenting TGO surface curvedness with respect to cracks location for 80 hours sample

Figure 4-5 b presents the curvedness of the surface that is equal to zero over the peaks and is maximum on the maximum slopes. To further analyze the location of the cracks versus the TGO asperities figure 4-6 is provided for the sample (d) (with size of 3 by 3 mm) which is thermally cycled for 80 hours. It can be seen that cracks in TBC are located above the summits or over a valley of the TGO and so the curvature map image shows not systematic relationship of crack to the subsurface. . There are also some few cracks that penetrated into the TGO. In figure 4-6 shows a 3D rendering of the crack shown in figure. By carful repeated viewing of these images when rendered in 3D there appears to be no systematic relation between the bond coat geometry and crack location. In addition the cracks are nearly always standing above the interface by a distance that is roughly in the range of between 20-50 microns or about 30 to 70% of the peak to valley height of the typical asperity.

Examination of Figure 4.5a it can be see that some larger cracks grow very little between 80 and 140 cycles while some smaller cracks overtake and become bigger than some large cracks. In crack growth modeling larger cracks will either grow faster or at the same speed as smaller cracks so the current findings are an important challenge to modeling efforts and again suggest very heterogeneous conditions in the TBC.

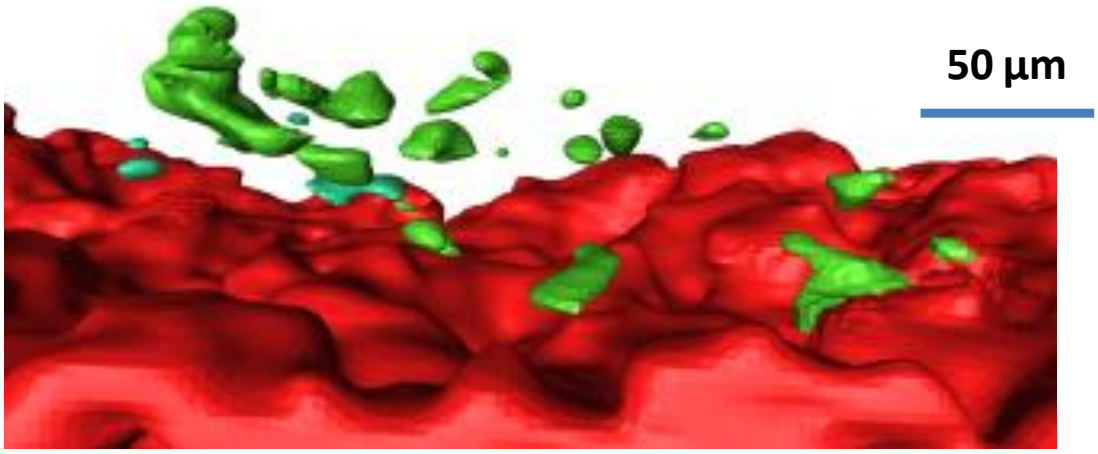

Figure 4-6 – Side view of cracks on sample (d) after 80 hours of thermal cycling at 1121

On this specific sample we can see 14 cracks. It can be seen that after about another 25 percent of life thermal cycling the cracks are linked in the following way.

- 14 cracks are reduced to 5 cracks and 5 new cracks are generated after the second round of cycling. Fourteen cracks merged into one in this case.
- All of the cracks are linked to each other in the last round of cycling before failure and generated 2 large cracks.
- After looking at the location of the cracks both on the segmented images and also virtual slices, which are like micrographs, cracks are found to be located above the TGO surface with a distance of about 20 to 60 micron from the TGO surface.

4.2 Cracks behavior

In all images the cracks are located right above the TGO up to about50-70 micron. Cracks appear and link in this area, but as it is getting closer to the TGO the crack progress and crack growth rate is generally higher. In figure 6 it is shown that although there is a larger crack above TGO a second crack marked by the arrow that is initially smaller grows faster and results in the

final failure. This is contrary to the expectations of fracture mechanics since the large crack that started presumably in a high stress area is out raced by a later appearing cracks that must grow faster than the big crack to catch up and pass it. The stress field in this case and/or the materials strength must be very heterogeneous or it evolves in a surprising way.

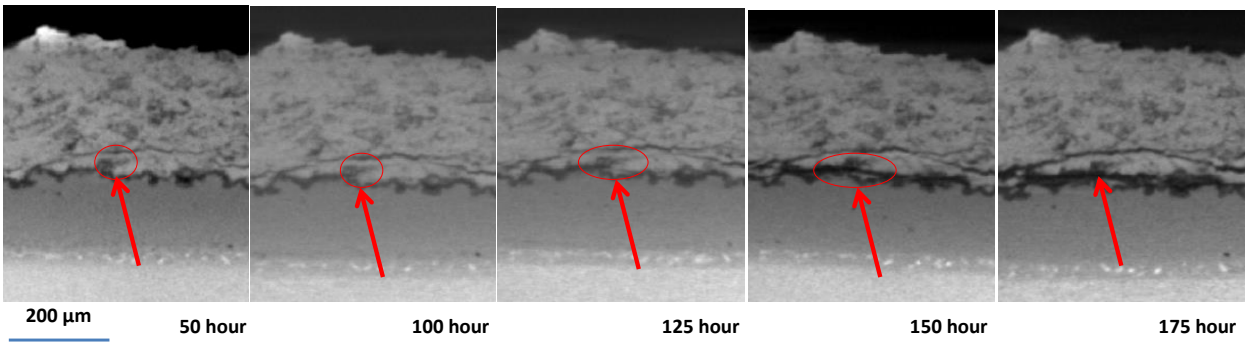

Figure 4-7– Faster crack growth seen in area closer to TGO

In addition to the crack tendency to grow in the region right above the TGO, it was also found that cracks, which are initiated between two peaks, will usually link to the TGO near the top of the TGO/bond coat peaks on the side. Crack initiation between peaks and merging into the TGO at the peak is show in Figure s which is for sample c, 1 by 2 mm sample.

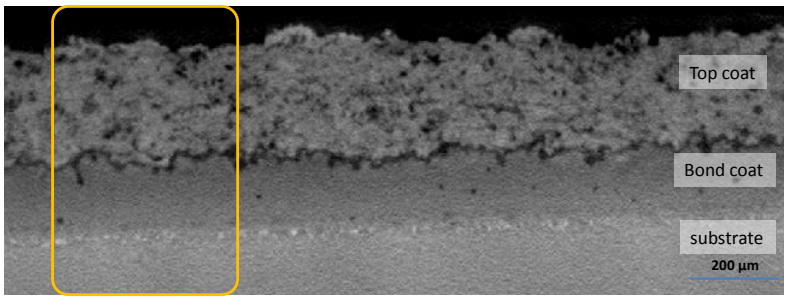

a) 150 hour cycled

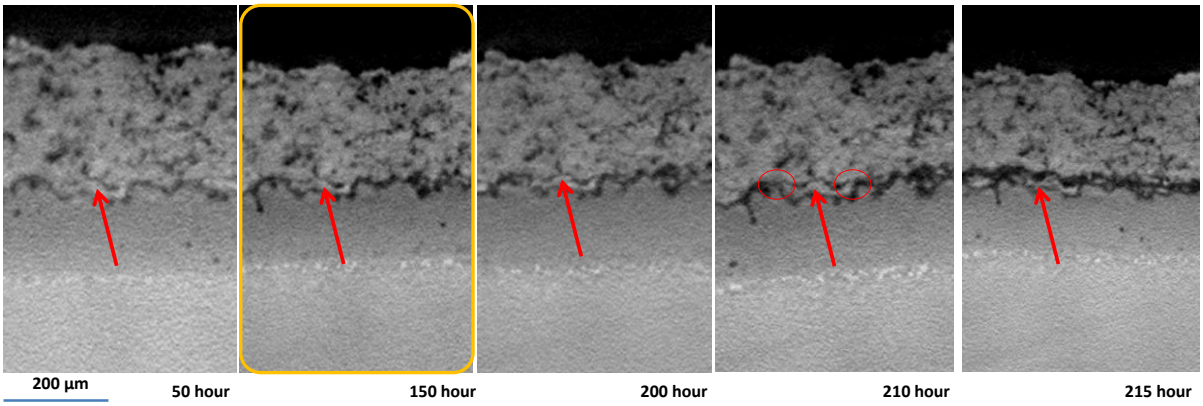

Figure 4-8– Crack linking to the TGO grown at top of the peaks

Quantification of cracks behavior is done by measuring the crack length and opening as well as the TGO thickness using the images from X-ray scans. Figure 4-9 gives the values for the crack lengths, crack density, TGO thickness and crack opening in sample type (c).

As it is seen in figure 4-8 cracks behavior can be quantified from the X-ray tomography data. TGO thickness and crack opening are also quantified using the micrographs and presented in figure graphs (a) and (b). In graph (d) the crack density is presented for every 2 millimeter of bond coat length which is the size of the tomography window. It can be seen that crack numbers are increasing as the sample is cycled up to about half of its life and decrease after that until failure. Meanwhile the crack length, graph (c), is increasing through the whole life of the TBC. It

can be seen from such results that during cycling, the small cracks start to appear in TBC and grow. By the time sample passes approximately half of its life, crack length is increasing at a higher rate and crack numbers decrease. One can conclude that crack linking dominates as the sample is cycled more than half of its life. Looking further to the results of graph (c), it shows that the sample type (c) which is only 2 mm wide has largest cracks during thermal cycling. Edge effect issue can be the main reason for large cracks in this sample in its early stages. Sample (d) and (e) which are 3 and 5 mm wide respectively behave almost same as each other which means a 3 by 3 mm sample is large enough to avoid edge effect issue and crack size is below 100 micron before 80 percent of their lives. This behavior has been also reported before [52] for whole coupon samples revealed by intensive sectioning involving over 1000 micrographs. This shows that the minimum size for samples to cut and still get the same behavior of a whole coupon can be as small as 3 by 3 millimeter.

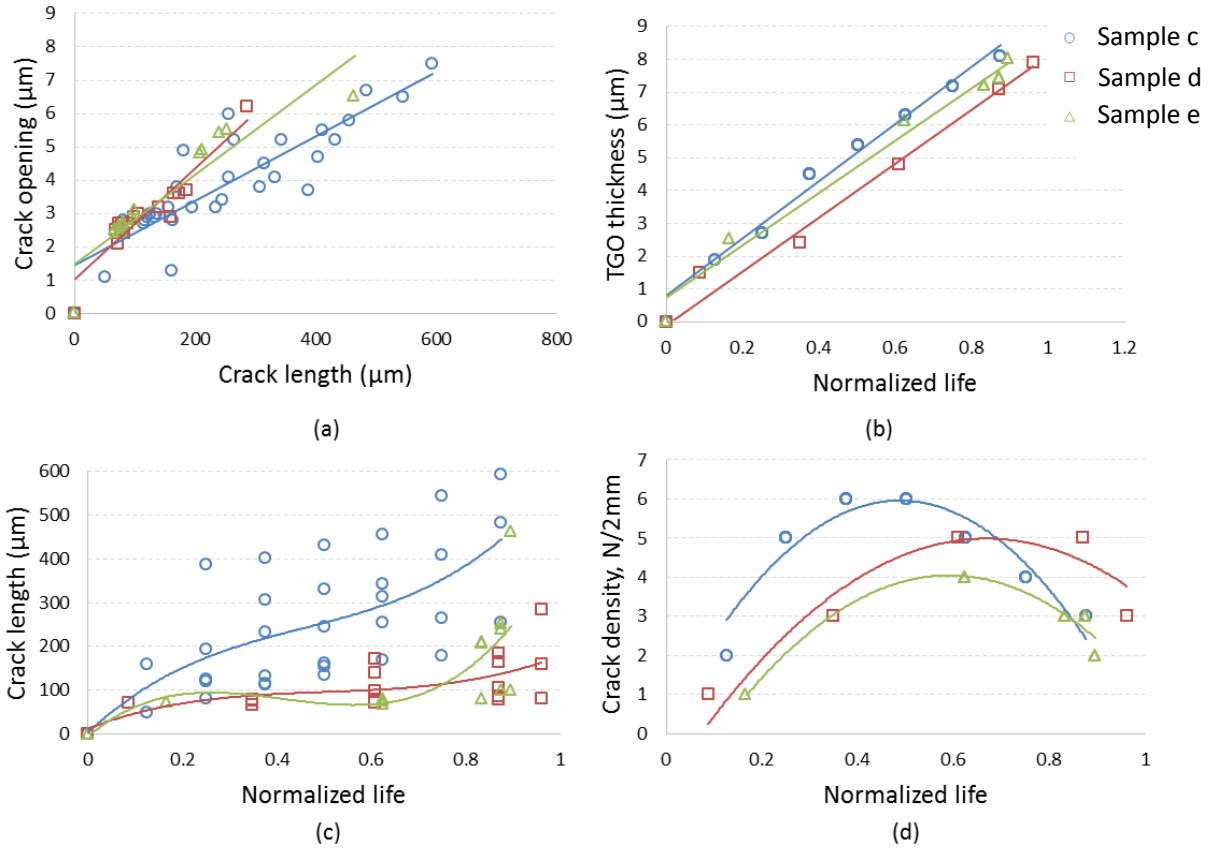

Figure 4-9– Quantified crack growth behavior

4.3 Crack correlation with TGO

Performing more than 1200 hours of tomography on more than 20 pieces of different size APS TBC samples, it was also found out that there is sometimes a correlation between the geometry of the crack and TGO in some locations. It is seen that these locations are mostly, where the crack is initially started over a peak and not in between or over a valley, Fig. 4-10.

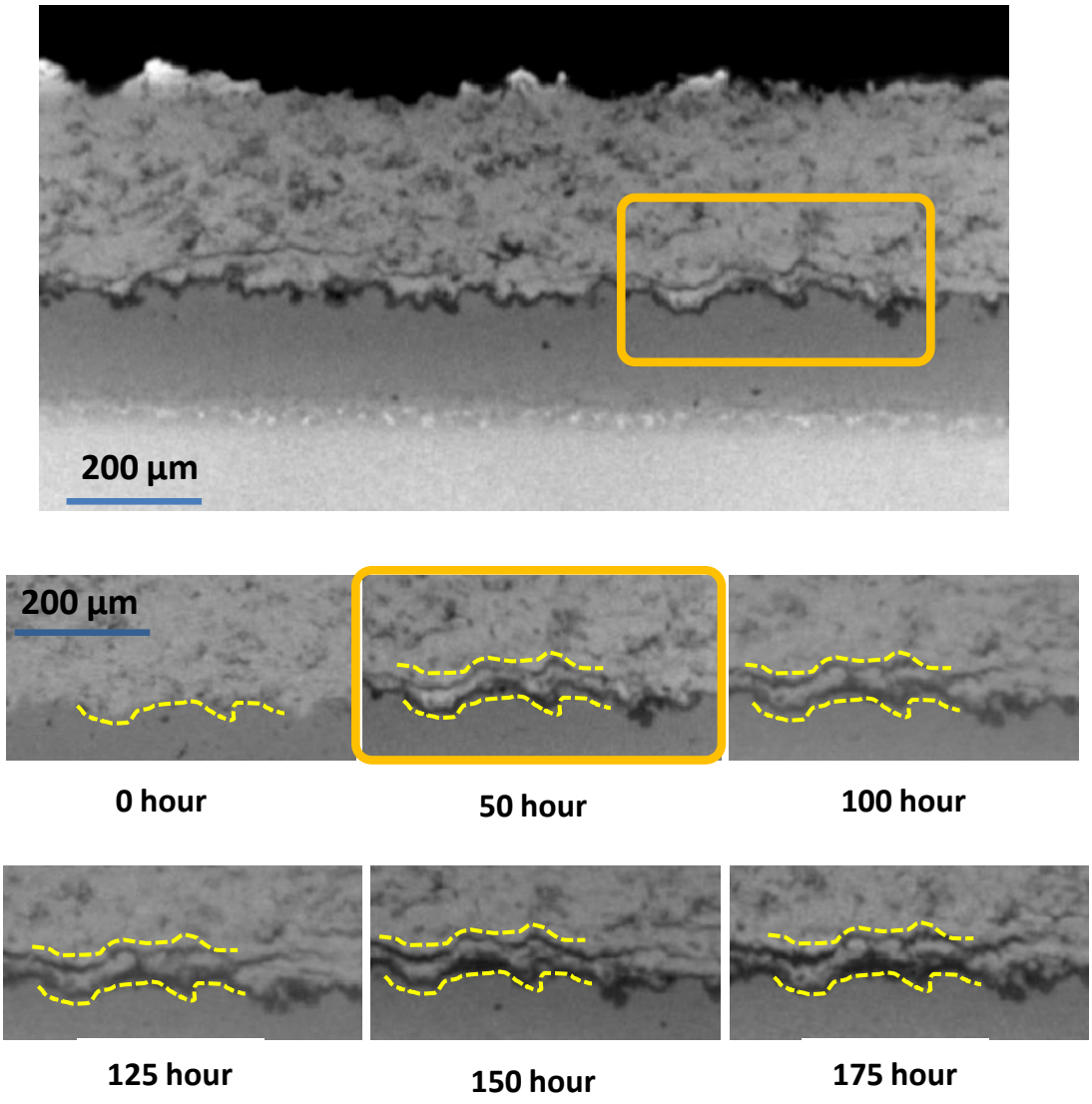

Figure 4-10-Correlation between crack and TGO seen in some specific areas

4.5 Correlation between bond coat and top coat surface geometry

According to the previous sections it is found out there is correlation between top coat and bond coat surface geometry which was done on a 100 micron thick top coat due to the limitations of the source power. Using the new source with 160 Kv power, it is possible to capture the surface parameters of the sample used in this research with 300 micron thick top coat. It is seen in figure

4-11 that the top surfaces can be separated virtually from the top coat and bond coat material and studied separately.

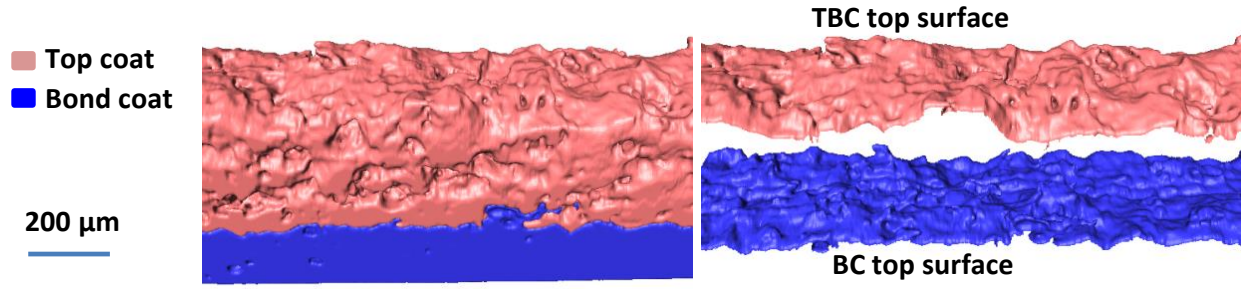

Figure 4-11– Top surface separation of TBC and BC for correlation analyses

Surface parameters can be analyzed using these kinds of data. Surface rumpling as one of the important causes of TBC failure is analyzed by calculating the tortuosity (the ratio of the TGO/bond coat interface length to its projected straight line length) for four different profiles selected from the surface. These four profiles are selected based on the surface characteristic wavelength, which is calculated based on the auto correlation and more details are out of the focus of this paper, in order to make sure they have the minimum dependency. It is seen based on figure 4-12 that tortuosity values both for bond coat and top coat are increasing as the sample is being thermally cycled. In contrast, the correlation value is decreasing during thermal cycling. The correlation is about 0.8 before thermal cycling which defines a considerable linear dependency between the two surfaces. This is nearly the same as reported on different samples in section 3.5. As the sample is getting cycled the correlation values is decreasing, which could be due to the reduction of connection between the two material as the cracks grow.

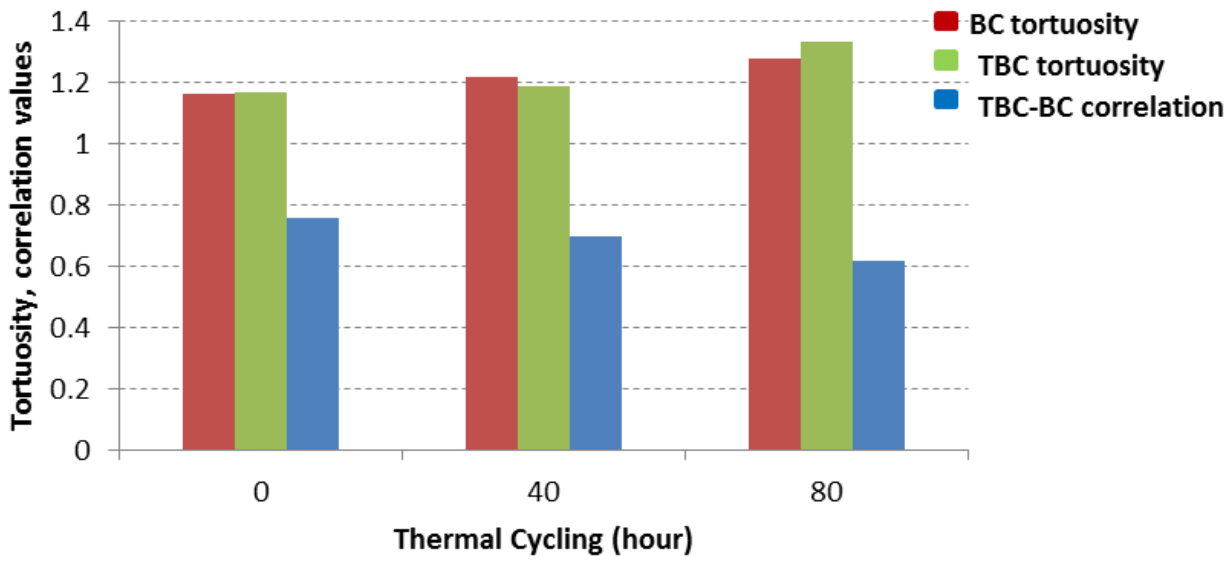

Figure 4-12– Tortuosity values for bond coat and top coat selected profiles and correlation between them

In addition to the correlation found between top coat and bond coat surfaces, it was also found out that this value is also dependent the thickness of the top coat. For a 100 micron thick top coat TBC the correlation is about 0.85 while it is just about 0.75 when the top coat is 250 micron thick. Although this values decreases with the top coat thickness but the correlation value is still considerable and can be used as nondestructive parameter for validation of bond coat rumpling.

Chapter 5 Conclusion and future work

This dissertation contributes to the study of thermal barrier coatings in five major areas:

1. **Confocal microscopy used to visualize crack shapes but due to the limited laser penetration into the TBC material this effort did not provide satisfactory results.**
2. **Optimizing the X-ray Tomography technique and its interdependent acquisition parameters for 3D imaging of thermal barrier coatings**

Making 3-D images using X-ray tomography is difficult due to the strong absorption of X-rays by the metal and ceramic samples. Parameter optimization is somewhat dependent on the x-ray hardware used. However the conditions found in this study are typical of adequate conditions and can be related to other hardware with basic knowledge of x-ray imaging physics. The specific machine used was the Versa 510 with a source voltage of 160 KV, a total power of 10 watts and an imaging device with 1 million pixels and various objectives. This major task was realized by several subtasks including:

- It was determined that maximum voltage of 160 Kv and maximum power were optimal for this machine. It could not be determined if higher voltages or power were more optimal due to machine limitations
- Optimizing the required number of X-ray projections to yield results that have the sufficient resolution to investigate regions of interests in the TBCs including TGO surface geometry and Voids in the ceramic top coat using 2000 projections. Crack imaging required 4000 projections. The number of projections was adequate while not being excessive to create artifacts due to the potential sample and stage motion or source energy instability.

- Optimizing the distance of the detector to the sample at 20 mm while the sample to detector distance was optimized at 30 mm to utilize simultaneous geometric and optical magnification to achieve the required pixel size previously selected based on investigating SEM images for cracks and stereo-photogrammetry for rumpling

3. Determining the correct sample size to make imaging TBC and further segmentation feasible

- TBCs are made of highly X-ray attenuating materials making it impossible for samples in the form of large coupons to be investigating. Smaller samples may behave differently and have different failure mechanism. This study has identified the ideal sample size which behaves similarly to that of a coupon for the first time by finding reduced sample sizes that yielded approximately the same cyclic furnace life and failure mechanism as larger coupons. This minimum sample size determination is somewhat dependent on the coating thickness and other properties but should allow excellent first choices to be made in future studies. In this study the minimum sample size was found to be 3 mm X 3 mm with the sample at full thickness. Smaller samples did not have the same life as full suzed samples and could not be used. The ideal sample size can be adopted by the community for further qualitative and quantitative studies of TBCs.

- **Developing Image Processing and Image analysis procedure to faithfully transfer 3D images to STL surface files as an enabling technology for any future 3D quantitative analysis**

- 2D quantitative data and qualitative analyses are possible by looking at 3D images but extracting 3D data requires segmentation, that is assigning a particular materials to each voxel based on the intensity value
- Challenges for segmenting TBCs are identified. In particular one has to be able to distinguish between pores and cracks and make sure the depth information of cracks is not exaggerated. This study uses localized range limited thresholding as opposed to automatic volume thresholding to assign pixel intensities belonging to the cracks only. In the selection of the threshold care must be taken to not count voxels partially covered by the crack to be labeled as part of the crack in order to not have cracks labeled as voids. The developed algorithm can be used in identifying cracks and segmenting them in 3D images from any other samples regardless of material.
- To utilize 3D visualization tools in AVISO the voxel (the TXM files) were converted to surface data files (.SURF files). Examination and understanding of the 3D images required this conversion. Also these types of generated data for surfaces can be directly imported in FE software or used for in modeling in future work by follow on students.

4. Proving the feasibility of the potential studies listed in (2) by performing quantitative (for the first bullets below) and qualitative (for the last 2 bullets below) analyses on more than 50 samples over time:

- It has shown that by adopting two registration measures one before acquisition and one after acquisition, one can make the technique repeatable enough to study evolution of a selected region of interest over several heat treatment intervals.
- This is an enabling technology which for the first time offers the unique opportunity to the community to track changes in different layers such as TGO, Bondcoat and Topcoat and cracks nondestructively and locally.

Specific crack characteristics were discovered

- **Crack shapes are highly irregular especially when they are larger and formed primarily by linking. In some cases they are not even simply connected.**
- **Initial crack span a range of aspect ratios for early cracks less than 50 microns the aspect ratio averaged 1.5 while for larger cracks the average aspect ratio was approximately 3.0 and values as large as 5 were observed.**
- **Crack linking involves intensive multiple linking events between cracks of a wide range of sizes. In as little a span as from 50 to 70% of the cyclic life, as many as 2-10 cracks can be linked into a single crack. It is likely that linking produces the highly irregular crack shape seen for larger cracks.**
- **Larger cracks do not necessarily grown faster than smaller cracks. Crack linking seems to lead to the faster growth instead.**

- **Cracks tend to grow about 25-50 micron above the TGO surface. This is between 0.5 and 0.8 times the typical asperity height**
- **The shape change of the bond coat is partially reflected in corresponding but somewhat smaller changes in the top surface of the top coat. This offer the possibly chance to look at rumpling damage from the free surface.**

The five initial questioned asked in the abstract are answered as following based on the above findings:

a) **Is the crack initiation location correlated with the initial bond coat TBC interface geometry?** It appears not to be strongly related to the shape of the underlying bond coat geometry especially for shorter cracks. This is not too surprising because the vast majorities of cracks are significantly above the bond coat summits and would appear in most cases too far away from the bond coat for it to have a dominant effect. This contradicts virtually all know models.

b) **What the shapes of TBC cracks are as needed for modeling?** In the early stages cracks range from near circular to having aspect ratios up to 4 Fig. 4.5a. There appears to be very heterogeneous behavior at this size scale. At later stages cracks have extremely irregular shapes and in some cases are not even simply connected 4.5b and 4.6. These shapes are quite surprising and are a big challenge derives such shapes from modeling unless linking is better understood.

c) **Does the largest crack grow equal or faster than the smaller cracks?** This is somewhat obscured by linking however there are many cases of small cracks growing much faster than large cracks again indicating highly heterogeneous material properties

or stress at the smaller size scales. This is not consistent with fracture mechanics assuming homogeneous material behavior and toughness.

d) **Crack linking is known to be a feature of the damage, what is the nature of the linking progression?** The linking is very rapid and in as little as at 20% interval of the failure life as many as 14 cracks can merge into a single large crack. In addition new cracks appear in the same time frame as the intense linking occurs (Fig. 4.5a) Cracks originally many diameters apart can merge in this relatively short time.

e) **What is the relationship between the geometry change at the hidden bond coat to ceramic interface and the ceramic free surface and can the free surface geometry change that is more easily measured be used to assess the extent of bond coat interface geometry?** The topcoat geometry changes is correlated with but less than that of the bond coat for the thickness studied here (250 microns) but measurement of bond coat surface geometry may be useful in non-destructive inspection.

Future Work:

As the entire process of imaging, post processing and analyzing has been optimized and verified in this work. The data provide TBC research with a treasure trove of information which enables numerous future studies:

- **Study the very early crack initiation and growth and more details of linking.**
- In the initial experiments the frequency of image acquisition needed to investigate behavior of interests had be guessed at from the results presented there is a need to take more frequent images beginning at about 15% of the life 50% of the life to

investigate the progression of linking in single events and to see where the early cracks form and estimate their growth rate.

- **Quantitative investigation of crack initiation correlation with the surface geometry of TGO**
- **Investigation of the dependence or independence of crack growth to crack area**
- **Finding the relationship if any between early crack initiation locations and the preexisting bond coat topography and/or the rumpling induced changes in that topography. This then can be compared to the assumptions made in existing models in the literature, suggesting which if any are matching the observed behavior and what the suggests is critical in modeling crack initiation locations.**
- **Current models based on assumed homogeneous material properties seem incapable of predicting the heterogeneous behavior observed. After or before developing an understanding of the nature of the heterogeneous behavior stochastic models will need to be made to predict the observed behavior.**

Chapter 6 References

[1] A. Kulkarni, A. Goland, H. Herman, A. J. Allen, T. Dobbins and F. DeCarlo et al, "Advanced neutron and X-ray techniques for insights into the microstructure of EB-PVD thermal barrier coatings," ,

[2] R. Panat and K. J. Hsia, "Experimental investigation of the bond-coat rumpling instability under isothermal and cyclic thermal histories in thermal barrier systems," *Proceedings of the Royal Society A: Mathematical, Physical and Engineering Sciences,* vol. 460, no. 2047, pp. 1957-1979, 2004.

[3] F. Wu, E. Jordan, X. Ma and M. Gell, "Thermally grown oxide growth behavior and spallation lives of solution precursor plasma spray thermal barrier coatings," *Surface and Coatings Technology,* vol. 202, no. 9, pp. 1628-1635, 2008.

[4] Y. Sohn, J. Kim, E. Jordan and M. Gell, "Thermal cycling of EB-PVD/MCrAlY thermal barrier coatings: I. Microstructural development and spallation mechanisms," *Surface and Coatings Technology,* vol. 146, pp. 70-78, 2001.

[5] B. Mendis and K. Hemker, "Thermal stability of microstructural phases in commercial NiCoCrAlY bond coats," *Scripta Materialia,* vol. 58, no. 4, pp. 255-258, 2008.

[6] A. Khan and J. Lu, "Behavior of air plasma sprayed thermal barrier coatings, subject to intense thermal cycling," *Surface and Coatings Technology,* vol. 166, no. 1, pp. 37-43, 2003.

[7] C. Mercer, D. Hovis, A. Heuer, T. Tomimatsu, Y. Kagawa and A. Evans, "Influence of thermal cycle on surface evolution and oxide formation in a superalloy system with a NiCoCrAlY bond coat," *Surface and Coatings Technology,* vol. 202, no. 20, pp. 4915-4921, 2008.

[8] H. Zhu, N. Fleck, A. Cocks and A. Evans, "Numerical simulations of crack formation from pegs in thermal barrier systems with NiCoCrAlY bond coats," *Materials Science and Engineering: A,* vol. 404, no. 1-2, pp. 26-32, 2005.

[9] T. Xu, S. Faulhaber, C. Mercer, M. Maloney and A. Evans, "Observations and analyses of failure mechanisms in thermal barrier systems with two phase bond coats based on NiCoCrAlY," *Acta Materialia,* vol. 52, no. 6, pp. 1439-1450, 2004.

[10] R. Wu, X. Wang and A. Atkinson, "On the interfacial degradation mechanisms of thermal barrier coating systems: Effects of bond coat composition," *Acta Materialia,* vol. 58, no. 17, pp. 5578-5585, 2010.

[11] V. Tolpygo and D. Clarke, "On the rumpling mechanism in nickel-aluminide coatings," *Acta Materialia,* vol. 52, no. 17, pp. 5115-5127, 2004.

[12] V. Tolpygo and D. Clarke, "Rumpling induced by thermal cycling of an overlay coating: the effect of coating thickness," *Acta Materialia,* vol. 52, no. 3, pp. 615-621, 2004.

[13] V. Tolpygo and D. Clarke, "Surface rumpling of a (Ni, Pt) Al bond coat induced by cyclic oxidation," *Acta Materialia,* vol. 48, no. 13, pp. 3283-3293, 2000.

[14] V. Tolpygo and D. Clarke, "On the rumpling mechanism in nickel-aluminide coatings (1)," *Acta Materialia,* vol. 52, no. 17, pp. 5129-5141, 2004.

[15] V. Tolpygo and D. Clarke, "Rumpling of CVD (Ni,Pt)Al diffusion coatings under intermediate temperature cycling," *Surface and Coatings Technology,* vol. 203, no. 20-21, pp. 3278-3285, 2009.

[16] V. Tolpygo and D. Clarke, "Temperature and cycle-time dependence of rumpling in platinum-modified diffusion aluminide coatings," *Scripta Materialia,* vol. 57, no. 7, pp. 563-566, 2007.

[17] S. Dryepondt, J. R. Porter and D. R. Clarke, "On the initiation of cyclic oxidation-induced rumpling of platinum-modified nickel aluminide coatings," *Acta Materialia,* vol. 57, no. 6, pp. 1717-1723, 2009.

[18] S. Sridharan, L. Xie, E. H. Jordan, M. Gell and K. Murphy, "Damage evolution in an electron beam physical vapor deposited thermal barrier coating as a function of cycle temperature and time," *Materials Science and Engineering: A,* vol. 393, no. 1-2, pp. 51-62, 2005.

[19] L. Xie, Y. Sohn, E. H. Jordan and M. Gell, "The effect of bond coat grit blasting on the durability and thermally grown oxide stress in an electron beam physical vapor deposited thermal barrier coating," *Surface and Coatings Technology,* vol. 176, no. 1, pp. 57-66, 2003.

[20] M. Wen, E. H. Jordan and M. Gell, "Effect of temperature on rumpling and thermally grown oxide stress in an EB-PVD thermal barrier coating," *Surface and Coatings Technology,* vol. 201, no. 6, pp. 3289-3298, 2006.

[21] R. Panat, K. J. Hsia † and J. Oldham, "Rumpling instability in thermal barrier systems under isothermal conditions in vacuum," *Philosophical Magazine,* vol. 85, no. 1, pp. 45-64, 2005.

[22] S. Dryepondt and D. R. Clarke, "Cyclic oxidation-induced cracking of platinum-modified nickel-aluminide coatings," *Scripta Materialia*, vol. 60, no. 10, pp. 917-920, 2009.

[23] J. Curran and T. Clyne, "The thermal conductivity of plasma electrolytic oxide coatings on aluminium and magnesium," ,

[24] Y. Zhao, A. Shinmi, X. Zhao, P. Withers, S. V. Boxel and N. Markocsan et al, "Investigation of interfacial properties of atmospheric plasma sprayed thermal barrier coatings with four-point bending and computed tomography technique," ,

[25] W.A. Ellingson, R.J. Visher, R.S. Lipanovich, and C. M. Deemer, "Optical NDE methods for ceramic thermal barrier coatings" *Journal of the American Society for Nondestructive Evaluation*, pp, 1-17, Nov. 2005]

[26] S. O. Chwa and A. Ohmori, "Microstructures of ZrO2-8wt.%Y2O3 coatings prepared by a plasma laser hybrid spraying technique," *Surface and Coatings Technology*, vol. 153, pp. 304-312, 2002.

[27] S. Shahbazmohamadi, E.H. Jordan, '"Optimizing an SEM-based 3D surface imaging technique for recording bond coat surface geometry in thermal barrier coatings," *Measurement and Science Technology*, pp. 1-12, 2012.

[28] Padture, Nitin P., Maurice Gell, and Eric H. Jordan. "Thermal barrier coatings for gas-turbine engine applications." *Science* 296.5566 (2002): 280-284.

[29] Vassen, R., Cao, X., Tietz, F., Basu, D., & Stöver, D. (2000). Zirconates as new materials for thermal barrier coatings. *Journal of the American Ceramic Society*,*83*(8), 2023-2028.

[30] Rabiei, A. G. E. A., and A. G. Evans. "Failure mechanisms associated with the thermally grown oxide in plasma-sprayed thermal barrier coatings." *Acta materialia* 48.15 (2000): 3963-3976.

[31] Miller, Robert A. "Thermal barrier coatings for aircraft engines: history and directions." *Journal of Thermal Spray Technology* 6.1 (1997): 35-42.

[32] Ellingson, W. A., Visher, R. J., Lipanovich, R. S., & Deemer, C. M. (2006). Optical NDE methods for ceramic thermal barrier coatings. *Materials evaluation*,*64*(1), 45-51.

[33] Tolpygo, V. K., & Clarke, D. R. (2000). Surface rumpling of a (Ni, Pt) Al bond coat induced by cyclic oxidation. *Acta Materialia*, *48*(13), 3283-3293.

[34] Zhao, Y., Shinmi, A., Zhao, X., Withers, P. J., Van Boxel, S., Markocsan, N., ... & Xiao, P. (2012). Investigation of interfacial properties of atmospheric plasma sprayed thermal barrier coatings with four-point bending and computed tomography technique. *Surface and Coatings Technology*, *206*(23), 4922-4929.

[35] Padture, N. P., Schlichting, K. W., Bhatia, T., Ozturk, A., Cetegen, B., Jordan, E. H., ... & Osendi, M. I. (2001). Towards durable thermal barrier coatings with novelmicrostructures deposited by solution-precursor plasma spray. *Acta materialia*, *49*(12), 2251-2257.

[36] Asadizanjani, Navid, Shahbazmohamadi, Sina, and Eric H. Jordan. "Investigation of surface geometry change in thermal barrier coatings using computed X-ray tomography." *38th Int'l Conf & Expo on Advanced Ceramics & Composites (ICACC 2014).*

[37] Feser, M., Gelb, J., Chang, H., Cui, H., Duewer, F., Lau, S. H., ... & Yun, W. (2008). Sub-micron resolution CT for failure analysis and process development.*Measurement science and technology*, *19*(9), 094001.

[38] Sunna, A., Hunter, L., Hutton, C. A., & Bergquist, P. L. (2002). Biochemical characterization of a recombinant thermoalkalophilic lipase and assessment of its substrate enantioselectivity. *Enzyme and microbial technology*, *31*(4), 472-476.

[39] Padture, Nitin P., Maurice Gell, and Eric H. Jordan. "Thermal barrier coatings for gas-turbine engine applications." *Science* 296.5566 (2002): 280-284.

[40] Ellingson, W. A., Visher, R. J., Lipanovich, R. S., & Deemer, C. M. (2006). Optical NDE methods for ceramic thermal barrier coatings. *Materials evaluation*,*64*(1), 45-51.

[41] Singh, H., & Gokhale, A. M. (2005). Visualization of three-dimensional microstructures. *Materials characterization*, *54*(1), 21-29.

[42] Dryepondt, S., Porter, J. R., & Clarke, D. R. (2009). On the initiation of cyclic oxidation-induced rumpling of platinum-modified nickel aluminide coatings. *Acta Materialia*, *57*(6), 1717-1723.

[43] Vaidyanathan, K., Jordan, E. H., & Gell, M. (2004). Surface geometry and strain energy effects in the failure of a (Ni, Pt) Al/EB-PVD thermal barrier coating. *Acta materialia*, *52*(5), 1107-1115.

[44] Chen, W. R., Archer, R., Huang, X., & Marple, B. R. (2008). TGO growth and crack propagation in a thermal barrier coating. *Journal of Thermal Spray Technology*, *17*(5-6), 858-864.

[45] Fan, X., Jiang, W., Li, J., Suo, T., Wang, T. J., & Xu, R. (2014). Numerical study on interfacial delamination of thermal barrier coatings with multiple separations. *Surface and Coatings Technology*, *244*, 117-122.

[46] Ranjbar-Far, M., Absi, J., Mariaux, G., & Smith, D. S. (2011). Crack propagation modeling on the interfaces of thermal barrier coating system with different thickness of the oxide layer and different interface morphologies.*Materials & Design*, *32*(10), 4961-4969.

[47] Miller, R. A., & Berndt, C. C. (1984). Performance of thermal barrier coatings in high heat flux environments. *Thin Solid Films*, *119*(2), 195-202.

[48] Eldridge, J. I., Spuckler, C. M., & Martin, R. E. (2006). Monitoring Delamination Progression in Thermal Barrier Coatings by Mid-Infrared Reflectance Imaging.*International journal of applied ceramic technology*, *3*(2), 94-104.

[49] Heeg, B., Tolpygo, V. K., & Clarke, D. R. (2011). Damage evolution in thermal barrier coatings with thermal cycling. *Journal of the American Ceramic Society*,*94*(s1), s112-s119.

[50] Ray, A. K., Roy, N., & Godiwalla, K. M. (2001). Crack propagation studies and bond coat properties in thermal barrier coatings under bending. *Bulletin of Materials Science*, *24*(2), 203-209.

[51] Cernuschi, F., Capelli, S., Bison, P., Marinetti, S., Lorenzoni, L., Campagnoli, E., & Giolli, C. (2011). Non-destructive thermographic monitoring of crack evolution of thermal barrier coating coupons during cyclic oxidation aging. *Acta Materialia*, *59*(16), 6351-6361.

[52] Ahmadian, S., & Jordan, E. H. (2014). Explanation of the effect of rapid cycling on oxidation, rumpling, microcracking and lifetime of air plasma sprayed thermal barrier coatings. *Surface and Coatings Technology*, *244*, 109-116.

[53] Jinnestrand, M., & Brodin, H. (2004). Crack initiation and propagation in air plasma sprayed thermal barrier coatings, testing and mathematical modelling of low cycle fatigue behaviour. *Materials Science and Engineering: A*, *379*(1), 45-57.

[54] Beck, T., Herzog, R., Trunova, O., Offermann, M., Steinbrech, R. W., & Singheiser, L. (2008). Damage mechanisms and lifetime behavior of plasma-sprayed thermal barrier coating systems for gas turbines—Part II: Modeling.*Surface and Coatings Technology*, *202*(24), 5901-5908.

[55] Chaimoon, K., Attard, M. M., & Tin-Loi, F. (2008). Crack propagation due to time-dependent creep in quasi-brittle materials under sustained loading.*Computer Methods in Applied Mechanics and Engineering*, *197*(21), 1938-1952.

[56] Chen, X., Hutchinson, J. W., He, M. Y., & Evans, A. G. (2003). On the propagation and coalescence of delamination cracks in compressed coatings: with application to thermal barrier systems. *Acta materialia*, *51*(7), 2017-2030.

[57] Xu, T., He, M. Y., & Evans, A. G. (2003). A numerical assessment of the durability of thermal barrier systems that fail by ratcheting of the thermally grown oxide. *Acta materialia*, *51*(13), 3807-3820.

[58] Aktaa, J., Sfar, K., & Munz, D. (2005). Assessment of TBC systems failure mechanisms using a fracture mechanics approach. *Acta materialia*, *53*(16), 4399-4413.

[59] Ahmadian, S., Thistle, C., & Jordan, E. H. (2013). Experimental and Finite Element Study of an Air Plasma Sprayed Thermal Barrier Coating under Fixed Cycle Duration at Various Temperatures. *Journal of the American Ceramic Society*, *96*(10), 3210-3217.

[60] Jinnestrand, M., & Sjöström, S. (2001). Investigation by 3D FE simulations of delamination crack initiation in TBC caused by alumina growth. *Surface and Coatings Technology*, *135*(2), 188-195.

[61] Sfar, K., Aktaa, J., & Munz, D. (2002). Numerical investigation of residual stress fields and crack behavior in TBC systems. *Materials Science and Engineering: A*, *333*(1), 351-360.

[62] Martena, M., Botto, D., Fino, P., Sabbadini, S., Gola, M. M., & Badini, C. (2006). Modelling of TBC system failure: Stress distribution as a function of TGO thickness and thermal expansion mismatch. *Engineering Failure Analysis*,*13*(3), 409-426.

[63] Białas, M. (2008). Finite element analysis of stress distribution in thermal barrier coatings. *Surface and Coatings Technology*, *202*(24), 6002-6010.

[64] Chang, G. C., Phucharoen, W., & Miller, R. A. (1987). Behavior of thermal barrier coatings for advanced gas turbine blades. *Surface and Coatings Technology*, *30*(1), 13-28.

[65] Xie, W., Jordan, E., & Gell, M. (2006). Stress and cracking behavior of plasma sprayed thermal barrier coatings using an advanced constitutive model.*Materials Science and Engineering: A*, *419*(1), 50-58.

[66] Ranjbar-Far, M., Absi, J., Shahidi, S., & Mariaux, G. (2011). Impact of the non-homogenous temperature distribution and the coatings process modeling on the thermal barrier coatings system. *Materials & Design*, *32*(2), 728-735.

[67] Ranjbar-Far, M., Absi, J., Mariaux, G., & Smith, D. S. (2011). Crack propagation modeling on the interfaces of thermal barrier coating system with different thickness of the oxide layer and different interface morphologies.*Materials & Design*, *32*(10), 4961-4969.